The Effects of Viscosity and Subsurface Heterogeneity on a Brine Barrier Approach to DNAPL Remediation

Lauren L. Murphy

A thesis presented to the faculty of the University of North Carolina at Chapel Hill in partial fulfillment of the requirements for the degree of Master of Science in the department of Environmental Sciences and Engineering, School of Public Health.

Chapel Hill
2006

Approved by:

Dr. Cass T. Miller

Dr. William G. Gray

Dr. Matthew W. Farthing

Abstract

Lauren L. Murphy: The Effects of Viscosity and Subsurface Heterogeneity on a Brine Barrier Approach to DNAPL Remediation
(Under the direction of Cass T. Miller)

Dense nonaqueous phase liquids (DNAPLs) are a long-term source of groundwater contamination. Difficulties of current remediation methods have led to the study of a novel brine barrier remediation technology (BBRT) which presents a solution to current limitations. This study utilized a mathematical model to advance understanding of BBRT at the macroscale. A subset of stochastic functions was employed to represent correlated random permeability fields and to asses their impacts on brine emplacement and brine removal efficiency.

The injection of a highly viscous brine into the subsurface was seen to cause a decrease in permeability, leading to brine mounding around injection wells. For moderately heterogeneous domains, this behavior was able to be mitigated by the use of sufficiently low injection rates. However, local heterogeneities were shown to be the dominant factor in subsequent brine removal, emphasizing the importance of subsurface knowledge for accurate modeling and efficient implementation of BBRT.

Acknowledgments

I would like to offer special thanks to my thesis committee—Cass Miller, William Gray and Matthew Farthing—for their support and guidance over the past two years. I feel grateful to have had the opportunity to learn from each throughout my experience at the University of North Carolina. I am particulary appreciative of the knowledge, patience, encouragement and time that Cass Miller has provided me.

I would like to thank Joseph Pedit for being willing to offer assistance and advice whenever the time arose. My friends and family have also been integral in the completion of this thesis. They have offered unwavering patience and support, for which I am grateful.

Contents

List of Tables

List of Figures

List of Abbreviations and Symbols

ACL	above the clay layer
BBRT	brine barrier remediation technology
$CaBr_2$	calcium bromide
DNAPL	dense nonaqueous phase liquid
DNTS	Dover National Test Site
HR	high rate
LF	lower flush
LR	low rate
MR	medium rate
NaCl	sodium chloride
PAH	polynuclear aromatic hydrocarbon
PCE	tetrachloroethylene
PDF	probability density function
REV	representative elementary volume
SGSIM	sequential Gaussian simulation
SRF	spatial random function
TCE	trichloroethylene
UF	upper flush
$C^{\iota a}$	salt concentration in the aqueous (M L^{-3})
$\mathbf{D}$	dispersion tensor (L^2 T^{-1})
$D_m^{\iota a}$	free liquid diffusion coefficient of salt in the aqueous phase (L^2 T^{-1})

$\mathbf{g}$	gravitational acceleration (L T^{-2})
$\mathbf{I}$	unit tensor (–)
$\mathbf{J}$	dispersive mass flux vector (M L^{-2} T^{-1})
k	intrinsic permeability of the porous media (L^2)
k_r^a	relative permeability for the aqueous phase (–)
l_i	scaling length parameter in the i^{th} dimension
p	phase pressure (M L^{-1} T^{-1})
p_c	capillary pressure (M L^{-1} T^{-2})
$\mathbf{q}$	Darcy velocity (L T^{-1})
S	external source or sink (M L^{-3} T^{-1})
S_w	saturation of the aqueous phase (–)
S_{wres}	residual saturation of the aqueous phase (–)
$\mathbf{v}$	phase velocity vector (L T^{-1})
α_L	longitudinal dispersivity (L)
α_T	transverse dispersivity (L)
ϵ	volumetric fraction (–)
λ_i	correlation length scale in the i^{th} dimension
μ	phase viscosity (M L^{-1} T^{-1})
ρ	phase density (M L^{-3})
$\boldsymbol{\tau}$	tortuosity tensor for porous media (–)
$\omega^{\iota a}$	mass fraction of salt in the aqueous phase (–)
superscript a	aqueous phase qualifier
superscript ι	salt species qualifier

1 Introduction

Over the last 25 years, the growing concern of hazardous waste sites within the United States has led to extensive research in the remediation of groundwater contamination. Dense nonaqueous phase liquids (DNAPLs) persisting in the subsurface continue to be one of the most difficult challenges to current removal techniques, and they are the most common class of contaminants found within the most severe of these sites, collectively referred to as Superfund sites [25]. In addition, DNAPLs, which include chlorinated solvents, such as trichloroethylene (TCE) and tetrachloroethylene (PCE), and polynuclear aromatic hydrocarbon (PAH) mixtures such as coal tar and creosote, are both a long-term source of groundwater contamination and a health risk to humans at low concentrations [25]. In spite of substantial research efforts, groundwater remediation techniques continue to be challenged by DNAPLs. Difficulties arise due to a variety of factors including subsurface heterogeneities, complex multiphase behavior, high DNAPL densities and viscosities, and slow transfer rates of DNAPL species to mobile phases. The quest for the least costly and most efficient and effective DNAPL remediation strategy thus remains a great environmental concern.

The importance and challenges of DNAPL removal in Superfund sites has in recent years led to the study of a novel remediation technique involving a dense brine solution, hereafter referred to as the brine barrier remediation technology (BBRT) [24, 29, 41]. The method is mobilization-based, as it relies on surfactant flushing to decrease capillary pressure trapping DNAPL in the pore space. However, the addition of a dense brine presents a solution to the difficulty of controlling the mobilized contaminant phase. BBRT has met with great success in laboratory experiments conducted to date, though topics requiring a more mature understanding remain. The motivation of this work was to acquire a better knowledge of BBRT at the macroscale by

numerically investigating two open issues—the effects of subsurface heterogeneity on the behavior of a dense brine solution and the viscous effects of brine.

Because of the inability to fully characterize subsurface properties, many groundwater flow and transport models make the assumption that porous medium properties are constant across the domain considered. Many studies of the consequences of this simplification are reported in relevant literature [14, 31, 38, 46, 52, 52, 53, 55–58], all of which have shown a large dependence of groundwater flow patterns on spatial variation in porous media. In addition, it has been determined that groundwater solute transport is primarily controlled by heterogeneity in the surrounding porous media and that the complexity of density dependent flow regimes is further complicated by subsurface variability [7, 57]. These findings, compounded by the vast amount of environmental issues requiring accurate groundwater flow models, have led to approaches of representing the spatial variability of porous medium characteristics, including continuous stochastic functions and various discrete paradigms.

The present study is aimed to utilize a subset of stochastic functions to numerically assess the impact of heterogeneity on brine behavior. Three-dimensional laboratory experiments investigating BBRT have accounted for subsurface variation, though a thorough investigation including many possible porous medium characteristics would be extremely costly and time consuming. Therefore, mathematical modeling of BBRT is potentially beneficial to improving the understanding of the processes involved in implementation.

Brine emplacement and recovery, two major stages of BBRT, were simulated using a domain representative of Dover National Test Site (DNTS), a field site in Dover, Delaware in which a pilot study of BBRT was conducted. Analysis was performed to evaluate the effects of heterogeneity on the efficiency and effectiveness of these processes. Also, it is hypothesized that, in addition to subsurface heterogeneity, the high viscosity of brines used in BBRT plays an important role in flow and transport. Further simulations were conducted to investigate this hypothesis. Analysis of simulation results is intended to create a stronger foundation for future

modeling and implementation of BBRT.

2 Background

2.1 Groundwater Remediation Strategies

Current groundwater remediation techniques can be classified by three major categories: (1) mass-transfer-based, (2) mobilization-based, and (3) reaction-based techniques.

2.1.1 Mass-transfer-based Techniques

In mass-transfer-based techniques, such as the pump-and-treat method and vapor extraction, the contaminant species is solubilized or volatilized to a mobile phase so that it can be extracted and treated. However, DNAPLs pose a challenge to these methods due to the contaminant species' slow mass transfer rates to a mobile phase [6, 12]. The pump-and-treat method involves the use of groundwater wells, which induce aqueous phase flow, to solubilize a contaminant phase and the subsequent extraction and treatment of the water. However, DNAPLs are only slightly soluble in water [6, 12], and DNAPL source zones create a reduction in permeability which causes water to flow around trapped DNAPL, reducing the compound solubilization rate seen in conditions without such by-passing [4, 12]. The reduction in permeability can be explained by the multiphase extension to Darcy's Law:

$$\mathbf{q}^{\alpha} = -\frac{k k_r^{\alpha}}{\mu^{\alpha}} \left(\nabla p^{\alpha} - \rho^{\alpha} \mathbf{g}\right) \qquad \text{for } \alpha = \text{aqueous phase, nonaqueous phase} \tag{1}$$

where $\mathbf{q}^{\alpha}$ is the Darcy velocity of the α phase, k is the intrinsic permeability of the medium, k_r^{α} is the relative permeability of the α phase, μ^{α} is the viscosity of the α phase, p^{α} is the pressure of the α phase, ρ^{α} is the density of the α phase, and $\mathbf{g}$ is a vector representing the acceleration of gravity. In the presence of DNAPLs, k_r^{α}, where α = the aqueous phase, decreases, as it is a function of the DNAPL saturation in the system [27]. This causes the aqueous phase flow velocity to decrease in the vicinity of DNAPLs. For this reason, among the others explained, the

pump-and-treat method requires long time scales for mass transfer and has thus been shown to be ineffective for DNAPL remediation [37].

Vapor extraction, another mass-transfer-based remediation technique, employs production wells to extract gas from the unsaturated zone. The pressure gradient created by the wells results in gas phase flow, and the vapor pressure of the species causes volatilization to the gas phase, where it can be removed and treated [12]. DNAPLs are relatively volatile, and so vapor extraction is useful in their extraction from the unsaturated zone [12, 39]. However, due to the dense nature of DNAPLs, most exist below the water table, making vapor extraction an ineffective remediation option.

2.1.2 Mobilization-based Techniques

In mobilization-based remediation techniques, a force imbalance is induced so that the capillary pressure causing contaminant pore entrapment can be overcome, causing the nonaqueous phase to mobilize. Some methods used to create a force imbalance include thermal methods and surfactant flushing. Thermal methods, the most common of which include steam heating and electrical resistive heating, are often employed and have been shown to be effective for organic chemicals [37]. Heating of the contaminants (including DNAPLs) often causes a reduction in viscosity and density, causing them to be less resistant to flow, and DNAPL volatilization rates increase as the boiling point is approached [37]. In addition, the compounds undergo a reduction in interfacial tension, which may lead to mobilization—allowing the contaminants to be extracted and treated [39].

Surfactant flushing employs compounds that act to reduce the interfacial tension between a non-mobile contaminant phase and the aqueous phase. Surfactants are injected into contaminated regions, and if they are able to decrease the interfacial tension to a state in which the capillary forces are dominated, then mobilization of the nonaqueous phase will occur [6, 12]. However, the risk common to any mobilization-based remediation method is the potential to con-

taminate previously uncontaminated areas due to the inability to control the newly mobilized phase.

2.1.3 Reaction-based Techniques

Reaction-based methods, including bioremediation and chemical oxidation, induce chemical reactions intended to convert a contaminant to a less harmful product. Chemical oxidation involves the addition of an oxidant, such as hydrogen peroxide, to a contaminated system. The oxidant is intended to induce a reaction which will oxidize the contaminant to a nontoxic product. However, chemical oxidation causes the depletion of naturally occurring organic carbon which results in a decrease in contaminant sorption sites and may ultimately lead to an increase in contaminant concentration [37].

Bioremediation methods are becoming increasingly popular for DNAPL contaminated areas, as they are able to enhance dissolution rates [37]. Bioremediation in a contaminated area is initiated by the creation or maintenance of an environment that is conducive to microbial growth. In turn, the microbes act to biodegrade the contaminant species. These techniques may cause daughter products that reduce the effectiveness of remediation; however, they may result in a continued contaminant reduction after treatment, as the microbial process persists. Reaction-based methods of DNAPL remediation are not optimal, as they require an initial transfer of the contaminant species to a mobile phase, posing the same problem as mass-transfer-based remediation methods [37].

2.2 Brine Barrier Remediation Technology

The dense brine approach to DNAPL remediation, an enhanced mobilization-based technique, offers a solution to the risk of contaminant spreading that is encountered with current methods. In a typical BBRT application, the injection of a brine more dense than a trapped DNAPL phase is intended both to affect the buoyancy forces, leading to the mobilization of DNAPL pools, and to act as a barrier for the vertical movement of the DNAPL species.

In the first stage of BBRT, a brine barrier is systematically established on top of a low permeability layer and is intended to assist in mobilization of a DNAPL phase. The addition of the dense brine results in an increase in buoyancy forces which may act to overcome the capillary forces causing DNAPL pools to persist in the saturated zone. In addition, DNAPL pools that have settled on the low permeability layer may float above the denser brine due to the change in buoyancy forces.

After a brine barrier is established in a contaminated system, surfactants or cosolvents are added to enhance DNAPL mobilization. As the interfacial tension decreases, the dense contaminant phase is mobilized downward. The vertical migration of the DNAPL is impeded by the brine layer, which acts as a pooling surface. Thereafter, DNAPL mass is extracted from the surface of the brine barrier using production wells, and residual DNAPL can be removed using vapor extraction as a tertiary process. Following remediation, brine is extracted from the production wells and can be reconcentrated for future BBRT reuse.

One-, two- and three-dimensional laboratory experiments investigating remediation methods in conjunction with brine have shown promise of controlling DNAPL migration [15, 24, 29, 41]. Three-dimensional experiments conducted on heterogeneous porous media contaminated with TCE have been shown to remove greater than 99% of the DNAPL mass originally present in the system [29]. Nonetheless, topics requiring a more mature understanding remain, including (1) the effects of heterogeneity on brine emplacement and recovery, (2) surfactant composition effects, (3) the effects of heterogeneity on DNAPL pool formation, (4) gravity-, viscous- and dissolution-induced instabilities, (5) the movement of disconnected phases, and (6) the viscous effects of brine.

The motivation of this study was to acquire a better understanding of BBRT at the macroscale by numerically investigating two of these open issues: the effects of subsurface heterogeneity on the behavior of a dense brine solution, and the viscous effects of brine. Though the investigation of DNAPL behavior is crucial to the overall understanding of BBRT, the computer

simulations conducted in this study were intended to analyze a subset of the processes in BBRT, the behavior of brine, and thus a DNAPL phase was ignored. The following two sections give relevant background and further motivation for the analyses conducted.

2.3 Effects of Heterogeneity on Brine Behavior

Brine behavior in the subsurface is affected both by the complexities of density and viscosity dependent flow and by the effects of heterogeneity on groundwater flow and transport. Both topics have been widely studied, both independently and in conjunction with each other. The present study is aimed to determine the effects that heterogeneity may have on brine emplacement and recovery at the field-scale. To understand the phenomena that may result from the introduction of brine to the subsurface, a general knowledge of density dependent flow is advantageous. The following sections outline the basic principles of variable density flow and the impacts of subsurface heterogeneity thereon.

2.3.1 Density Dependent Flow

Groundwater systems may contain significant density variations, resulting from temperature changes, pressure shifts or changes in solute concentrations. Flow induced by the density gradient is referred to as density dependent flow and is seen in a variety of situations that are important to current environmental issues, including possible nuclear waste disposal beneath rock salt formations, dense contaminant migration, saltwater intrusion in aquifers, and geothermal energy production [57]. For these reasons, investigations of variably dense groundwater flow and transport are a great concern and have been given increased attention over the past 35 years [1, 10, 21, 23, 43, 53, 54].

Thorough numerical and laboratory investigations have shown some systems with density gradients as small as that between freshwater and seawater to result in complex flow patterns. Though these unusual flow fields do not occur for DNAPL systems in general, as most are dilute by nature, complexities do arise in certain DNAPL plumes. Therefore, the addition of a dense

brine phase to the subsurface is assumed to potentially generate complex flow behavior.

Density dependent flow occurs as a variably dense system tends toward a stable configuration, or a stratified density, and it has a significant effect on species transport [56, 57]. Concentration differences between dense plumes overlying fresh groundwater can cause free convection, or a downward flow, due to buoyancy and gravity forces. This convection, depending on the magnitude of the density difference, can lead to instabilities within the system, or downward and nonuniform protrusions of the dense plume. In addition, the combination of the free convection and hydraulically driven forced convection, or advection, can lead to hydrodynamic mixing, or complex circular flow patterns, which are often difficult to predict [10]. In density driven flow, this hydrodynamic mixing is usually seen to dominate molecular diffusion, as the amount of solute that becomes involved in mixing is generally much greater than that in diffusion, and mixing occurs more rapidly and over a much longer spatial scale than does diffusion [10, 52, 56, 57].

In addition to competition between buoyancy and dispersive forces in systems with dense fluid above less dense fluid, complexities arise from phenomena that occur due to the ability of a dense phase to occlude the pore space and block fluid flow. The resulting heterogeneity creates an effect referred to as fingering, in which less dense fluid creates a "finger" as it flows through more permeable regions more quickly than through the obstructed pore space. Though this effect has been mathematically described for a DNAPL phase [27, 28, 40], as has DNAPL transport, no three-dimensional model exists that can accurately simulate the flow of dense brine, DNAPL, and surfactant in a heterogeneous porous medium. Because the recovery phase of BBRT involves the displacement of brine by freshwater, which may lead to fingering, a model capable of predicting this phenomenon would be beneficial.

As the physical characteristics of density dependent flow are complex, it follows that modeling this behavior has proven to be challenging. Rayleigh, the pioneer in modeling density dependent flow, studied systems thermally heated from below and used mathematical analysis to determine the principles that describe the formation of density induced instabilities [48]. In

the 1970's, mathematical models of brine transport in porous media were first presented by Bear [3, 4] and have since been widely investigated on the applicability to high-concentration-gradient fluid flow [19, 20, 23, 35]. Much can be found within the literature on mathematical models [2, 21, 22, 54] and numerical simulations [1, 11, 42, 43, 45, 61] of systems with varying density, however none of which have comparable gradients to those necessary in BBRT.

Numerical and experimental observations of density dependent flow reported in the literature all involve density gradients much smaller than those in BBRT experiments using calcium bromide ($CaBr_2$), which has a density of 1.7 g mL^{-1}. Because of a limited knowledge of systems with such a large density variation, in addition to the differences that arise between lab-scale and field-scale phenomena, accurate models of brine emplacement and recovery are necessary to assist in field-scale experiments involving BBRT. Many intricacies of this task arise from complexities within the system, including density induced instabilities, and from the quantification of subsurface heterogeneity which has also been shown to affect density dependent flow and solute transport.

2.3.2 Effects of Heterogeneity on Flow and Transport

While the effects of density gradients on groundwater flow have been widely studied in recent years, so have the effects of heterogeneity in hydraulic properties of porous media on flow and transport [14, 31, 38, 46, 52, 52, 53, 55–58]. These properties include grain size, permeability, porosity and storativity, all of which are included in the basic conservation equations used to solve groundwater flow and transport problems. Studies involving spatial variability in intrinsic permeability or hydraulic conductivity have all shown groundwater flow and solute transport to be greatly dependent on changes in porous medium properties [57, 60]. In addition, investigations of the effects of heterogeneity on density dependent flow have demonstrated a dependence of instability onset and growth or decay on the magnitude of spatial variability in subsurface characteristics [57]. Various approaches used to account for subsurface variability and

the resulting effects on solute transport are discussed in §2.5.

2.4 Viscous Effects of Brine

An overwhelming majority of variable density groundwater flow and transport models make the assumption that the variation of fluid viscosity with concentration is negligible [44]. It is common practice in numerical studies to assume a constant viscosity equal to that of freshwater, as the effects of viscosity have been shown to depend on solute mass only in systems of high concentration. However, the exact level at which concentration differences should be regarded is uncertain and thus loosely defined.

Though various studies have been conducted, the result of neglecting viscosity changes remains questionable [44]. Fried stated that viscous effects can be neglected when the maximum salt concentration difference is that between freshwater and seawater [17]. In addition, Koch and Zhang used mathematical analysis to conclude that the effects of viscosity are negligible compared to the effects of density [33, 34]. They demonstrated that a viscosity difference of 5% would result in a velocity change of 5%; however, a similar variation could result from numerical or physical uncertainties. To investigate the implications of neglecting viscosity, Ophori conducted a numerical analysis of a system in which a horizontal pressure gradient created a force for fluid flow, where recharge and discharge were allowed at the domain's upper boundary. Using a freshwater saturated system as his baseline, and comparing to an initially density-stratified system, he concluded that the use of an unrealistically large viscosity value for a given concentration resulted in an overestimation of groundwater movement upward through the domain and an underestimation of recharge. Also, an insufficient value for viscosity resulted in the prediction of exaggerated groundwater sinking and recharge and an underestimation of groundwater floating [44].

The impact of viscosity variations on fluid velocities has been seen to cause "viscous fingering," or flow patterns similar to the density induced fingers described previously. Though

overall groundwater instability formation depends on gravity and viscous forces, and on subsurface heterogeneity, independent studies of viscous fingering are important, as this phenomenon could be the dominant mechanism of pattern formation in some quasi-homogeneous, low-density flow systems [30]. Investigations have shown complex flow patterns to arise as less viscous fluid displaces more viscous fluid. Finger-like protrusions arise due to velocity variations which result from viscosity differences between phases or among a single phase. In miscible systems, the complex flow patterns that ensue depend on viscosity variations and diffusive mixing. In immiscible systems with variable density and viscosity, instabilities form due to viscosity differences and gravity forces [26].

A typical brine solution used in BBRT contains much greater viscosity variations than those seen in most viscosity related studies. To contrast the representative difference used in Koch and Zhang's analysis, the viscosity of $CaBr_2$ is 600% of freshwater. Therefore, it is hypothesized that viscous effects must be considered to properly model brine transport in porous media, as they may have a significant effect on the velocity profile and may lead to viscous fingering. The following section details methods used to represent heterogeneity in the previously mentioned investigations, in addition to other popular approaches currently used.

2.5 Methods of Heterogeneity Representation

Porous media found within aquifers are inherently heterogeneous. However, since quantification of hydraulic characteristics is costly, time consuming and impractical across an entire domain, subsurface properties are often assumed to be constant in models used to simulate groundwater flow and transport. However, studies of the errors generated by this simplification have shown spatial variability in the subsurface to have a large effect on groundwater flow regimes and contaminant transport [38, 50, 52, 53, 55, 57]. In turn, many methods have been employed to attempt to account for this variability, including statistical covariance models, Markov chains, continuous distribution models and discrete random fields employing geostatistical approaches,

such as facies, layers or lenses [13, 31, 50, 57]. The effects of heterogeneity on flow and transport have been analyzed using analytical, numerical and experimental methods, each employing a variety of techniques to account for subsurface variability [31, 38, 52, 53, 55, 57]. Results conclude that the degree and type of heterogeneity in the subsurface greatly impact groundwater flow and transport.

2.5.1 Homogeneous Porous Media

Though subsurface properties are heterogeneous, accounting for spatial variation greatly increases the complexity of numerical simulations. For this reason, many groundwater flow and transport investigations make the assumption that porous medium properties are homogeneous. Heterogeneity, however, greatly impacts flow and transport in porous media, yet the use of a carefully chosen homogeneous model domain may result in adequate approximations of fluid flow and solute transport. This is the basis of equivalent porous media.

Equivalent porous media employs homogenization theory, or the idea that hydraulic properties are identical across a representative elementary volume (REV), which Bear defines as the smallest volume over which the governing equations of flow apply [3]. To quantify the subsurface of a domain as an equivalent porous media, one attempts to find an "effective hydraulic conductivity," or the single value of hydraulic conductivity that can best represent a heterogeneous domain. For the method to be accurate, the REV must be smaller than the major variations in hydraulic conductivity [13]. To test this method, the average hydraulic head at any point that is found from a stochastic solution must be equal to the value of hydraulic head found at that point using a deterministic solution that employs the effective hydraulic conductivity [58]. Once an effective value is found, it may be utilized to simplify any further analysis. The use of equivalent porous media models are able to fairly accurately predict flow patterns in the case of karst aquifers, which are highly heterogeneous and fractured [51]. However, a majority of systems are considered non-homogenizable, in which case, alternative measures must be taken

to represent subsurface heterogeneity.

2.5.2 Layered and Lenticular Porous Media

It is common to see a layering of geological media, as sedimentary structures are deposited over time. Many groundwater flow and transport analyses have accounted for subsurface heterogeneity by assuming stratified layers of homogeneous media, or layers with varying averages and variances [50]. A variation of layered media is the representation of porous media as lenticular, or comprised of lens shaped structures, each with different characteristics [50, 53]. This is often more representative than layering. As an example, an extensive investigation into the hydraulic conductivity in the well-studied Borden aquifer revealed the site to be comprised of many discontinuous lenses with different hydraulic properties [60].

McKibbin et al. experimentally studied thermal convection in heterogeneous media by representing the media with layers of homogeneous material [38]. Their findings suggested that as the number of layers increased, the flow system more closely resembled that found in a homogeneous domain. However, for systems of few layers, the velocity field became more dependent on the layer properties.

Schincariol and Schwartz also employed the idea of layering in experimental designs to investigate the migration of dense plumes in a freshwater saturated domain [53]. Using varying sizes of industrial glass beads to mimic subsurface layers and using sodium chloride (NaCl) to create a dense fluid, they were able to compare plume migration to that in homogeneous media. Within the experiments, density differences as low as 0.0008 g mL^{-1} were seen to produce gravitational lobe shaped instabilities beginning at the bottom of the plume. Differences of only 0.0015 g mL^{-1} produced convective mixing, which significantly altered the spreading process. Reductions of hydraulic conductivity of only a half order of magnitude led to changes in plume flow, sometimes resulting in plume velocities larger than ambient groundwater velocities, depending on the orientation of dipping layers. Although the dense plumes sank and convective

mixing occurred in both homogeneous and layered media, mass was seen to accumulate at layer interfaces in the heterogeneous media, forming mounds.

The complexity of the effects of heterogeneity was further demonstrated by the contradicting effects of dipping beds on advective spreading (sometimes causing enhancement and other times the opposite), explained by differences in the mean flow direction of ambient groundwater. As dense fluid mounded against low conductivity units, where the barrier to vertical flow was dipping, the density forces created a component of flow that was down the topographic gradient of the interface. If this component were in the same direction as the mean flow, then plume migration was enhanced. If, however, these directions were opposites, plume spreading was dissipated.

In addition to layered media, Schincariol and Schwartz were also able to represent lenticular media using glass beads [53]. Conducted to create benchmarks, experiments containing homogeneous porous media, showed that in flow with small density differences, local-scale dispersion effects and diffusion produced little mixing, which occurred only at the edge of the plume. In experiments with higher density gradients (the highest of which involved NaCl with a density of 1.0053 g mL^{-1}), vertical mixing occurred as a result of convective dispersion. However, when lenticular media were used, a combination of convective dispersion and nonuniform flow resulting from heterogeneities created a much more highly dispersed plume, and the density induced instabilities were dissipated by this dispersion. The spreading seen in lenticular media was much more complex than that seen in the homogeneous and layered experiments because falling instabilities were attracted into high conductivity lenses yet dissipated by low conductivity lenses. Some lenses inhibited vertical motion and instability development, and the plume experienced splitting around other lenses. Overall the plume experienced much greater mixing in the lenticular media experiment than in the layered media experiment as demonstrated by the fact that the densest plume took almost 7 times as long to reach the bottom of the tank in the former than in the latter.

2.5.3 Spatial Random Functions

The stochastic approach to representing subsurface heterogeneity employs statistical models to represent variables using spatial random functions (SRFs), with a given mean, variance, covariance structure, and correlation length scale. SRFs are undoubtedly the most widely employed method to represent heterogeneity, as they are well understood, verified to be fairly representative for certain domains and able to account for aggregate hydraulic properties as well as for spatial variability within. For slightly heterogeneous areas, data collection has shown that these statistical models are effective in the representation of hydraulic conductivity [18, 57, 60]. In addition, studies by Freeze, among others, have shown that hydraulic conductivity is often log-normally distributed [16, 57]; i.e., the probability density function of $ln\ K$, where K represents hydraulic conductivity, is normally distributed.

The objective of an SRF is to account for the fact that subsurface properties at points in space are correlated depending on their distance apart. To do so, a covariance model is used to create spatial random fields, and the flexibility of this method is found in the number of distinctive covariance models that are employed [50]. Because the true nature of the heterogeneity is uncertain, common stochastic analysis involves the solution of many equi-probable equations, of which the average result is assumed to be a good approximation of the solution. This concept is referred to as Monte Carlo analysis and is commonly employed in groundwater flow and transport studies.

Spectral methods represent spatial variability as a set of waves with different parameters, including wavelength of the periodic structure, mean value and amplitude, which accounts for the amount of variation around the average value [50]. Researchers have suggested that hydraulic properties can be well described by wave functions, such as sinusoidal distributions, and the use of such methods is very popular due to the mathematical advantages provided [50]. Not only can analytical solutions be more easily obtained, but the methodology introduces a technique to

find the limits of spatial resolution given a set of field data.

In 1998, Schincariol was the first to numerically study density dependent flow in heterogeneous porous media using correlated random permeability fields [52]. He demonstrated that the statistics of the permeability field, including its mean, variance and correlation length, were important factors in both the onset of density induced instabilities and the growth and decay of these instabilities. Also, local heterogeneity and the combination of low and high permeability layers were shown to be important in determining the extent of mixing and the size of instabilities. Schincariol's numerical tests surfaced a contradiction that although heterogeneities created initial plume perturbations, a greater heterogeneity and anisotropy led to a greater dampening of instability growths.

Simmons et al. also used a numerical model to study dense plume migration in spatially correlated permeability fields [57]. Though heterogeneity resulted in differing flow fields and plume migration, prediction seemed to be extremely difficult as the results were all greatly dependent on the cumulative distribution of high and low permeability regions. While areas of high permeability enhanced plume migration, sections of low permeability dissipated instabilities. Interestingly, in different heterogeneous systems with identical statistical properties, plume migrations differed drastically, though, in each, instabilities were dissipated by dispersive mixing. Through numerical simulations, Prasad and Simmons also found that randomly correlated permeability fields caused convective mixing, which reduced plume instabilities [46].

Utilizing spectral methods, Simmons et al. conducted a numerical study to determine if a relationship exists between permeability wavelength and the stability of a dense plume [57]. Stability was shown to be dependent on both the solute concentration and on the wavelength of heterogeneity. It was demonstrated that in a system with small concentration gradients (0.005 g mL^{-1}), larger permeability wavelengths were required to increase the plume instability, and as concentration differences were increased to 0.1 g mL^{-1}, smaller wavelengths were able to affect instabilities.

2.5.4 Multi-Scale Methods

Though the most common representation of subsurface variability is through the use of SRFs, these methods are not optimal for the quantification of heterogeneity at multiple scales. Because a great level of detail is needed to accurately represent heterogeneity, large scale simulations can be computationally intensive. However, the level of detail necessary varies across a domain, as a finer discretization is essential near wells or high conductivity lenses, but a coarser grid is sufficient in areas in which velocities are relatively uniform. To take advantage of this, a process referred to as upscaling can be performed [32, 50, 64, 65]. In this approach, an initially refined grid is coarsened in areas requiring less resolution. Blocks which are coarsened retain a "block-effective" property value based on values at the finer discretization [50]. Different methods for assigning block-effective conductivity are practiced. Some prefer the average of the flux and the gradient over a block, while others claim the block effective conductivity should result in the same value of energy dissipation as that seen with a refined mesh.

An additional method of accounting for multiple scale heterogeneity includes an extension to the Markov chain, a conditional probability model often used to represent a discrete variable, and therefore popular for modeling structures such as facies. The concept of facies begins with bedsets, which are created as sediment is deposited over time. A collection of bedsets which contain common physical characteristics is referred to as a lithofacies. A single lithofacies contains regions, or facies, which have distinct permeability patterns, and the accumulation of these facies is often represented by a Markov chain or a discrete spatial random function [50]. Though the Markov chain technique does not employ a variogram, it accounts for spatial correlation by employing conditional probabilities [14]. In random fields created using Markov chains, the value of the variable at one location depends only on its value at the previous location, i.e., the probability of a value at a location is conditioned upon the value at the previous location.

An advancement, proposed by Dekking et al., is a methodology to characterize subsurface

properties using an extension to Markov chains that portrays coarse to fine scale transitions in a variable [8]. The novelty of the technique, which is built on a changing scale representation of heterogeneity on trees, is the ability to account for multi-scale heterogeneity. Referred to as "tree index Markov chains," they are beneficial due to their ability to account for both stationary and nonstationary fields and to allow for conditioning on measured data.

For many heterogeneous domains, it is common to employ two or more methods of heterogeneity representation, as the subsurface is comprised of drastically different components. In research on alluvial fans, which are one such set of these nonuniform domains, Weissmann and Fogg use a transition probability/Markov geostatistical method, introduced by Carle and Fogg, which can incorporate hard data and can account for multi-scale heterogeneity by dividing the domain into separate "units" [5, 63]. The model determines the lengths, proportions and positions of facies probabilistically. This allows the alluvial fan to be represented as non-stationary.

Recent research has shown that geometry in the subsurface is often fractal in nature and thus can not be properly defined by classical geometry. In this case, flaws are generated by the use of multi-scale methods, including upscaling. Therefore, fractal models are being increasingly employed in groundwater flow and transport analysis. In a 2002 study, Lu et al. statistically analyzed a stochastic facies model that included both large differences in log permeability variation in each facies and large log permeability variations between facies. Analysis of overall values of permeability resulted in a distribution function that seemed physically improbable, and the researchers proposed an alternative heterogeneity model, which combined a fractal model and stochastic facies model. In this fractal/facies methodology, large-scale facies characteristics are generated with an indicator simulation, and fractal models are used to produce distributions within each facies. Analysis of the methodology, using sets of laboratory and field data, supports its validity for domains which can be divided into facies [36].

3 Methods

3.1 SUTRA Computer Model

All computer simulations in this study were conducted using SUTRA Version 2D3D.1, a model for saturated-unsaturated, variable-density groundwater flow with solute or energy transport. SUTRA is provided by the United States Geological Survey (USGS) and is available for download at http://water.usgs.gov/nrp/gwsoftware/sutra.html. The model simulates three-dimensional saturated or unsaturated density-dependent groundwater flow and transport using a hybrid finite-element mesh discretization and a finite difference time-stepping method to approximate the conservation of mass of a fluid and either the conservation of mass of a solute or the conservation of energy of a fluid [62]. The code solves for fluid pressures and concentrations as mass fractions as they change with time. As is true with all approximate, discretization-based groundwater modeling applications, the method is accurate only for problems posed with proper spatial and temporal discretizations. Related programs provided by the USGS and utilized in this report are SutraPrep Version 3D.1 pre-processing software and SutraPlot Version 2D3D.1 graphical post-processing software [47, 59].

The governing equations required to describe the flow of a single, yet variably dense, aqueous phase in porous media include the conservation of mass and momentum for the aqueous phase and the conservation of mass and momentum for salt within the aqueous phase. The conservation of mass and momentum for the solid phase can be ignored by assuming that the porous medium is immobile and incompressible. In the simulations conducted, mass exchange of the salt species from the aqueous phase to the solid phase was also ignored by making the common assumption that salt is nonadsorbing.

The conservation of mass for the aqueous phase can be written as:

$$\frac{\partial(\epsilon^a \rho^a)}{\partial t} + \nabla \cdot (\epsilon^a \rho^a \mathbf{v}^a) = S^a \tag{2}$$

where ϵ^a is the volume fraction of the aqueous phase (volume of the aqueous phase per volume of the domain), ρ^a is the density of the aqueous phase, $\mathbf{v}^a$ is the velocity vector of the aqueous phase, and S^a is any external aqueous phase source or sink.

For saturated flow, it is common practice for Darcy's Law to be used to account for the conservation of momentum of the aqueous phase. This is given as:

$$\mathbf{q}^a = \epsilon^a \mathbf{v}^a = -\frac{k}{\mu^a} (\nabla p^a - \rho^a \mathbf{g}) \tag{3}$$

where $\mathbf{q}^a$ is the Darcy velocity of the aqueous phase, k is the intrinsic permeability of the porous media, μ^a and p^a are the dynamic viscosity and pressure of the aqueous phase, respectively, and $\mathbf{g}$ is the gravitational acceleration vector. Note, in saturated conditions, ϵ^a is equal to the system's porosity.

The conservation of mass for a nonreactive, nonadsorbing salt within the aqueous phase can be written as:

$$\frac{\partial}{\partial t} (\epsilon^a \rho^a \omega^{\iota a}) + \nabla \cdot (\epsilon^a \mathbf{v}^a \rho^a \omega^{\iota a} + \mathbf{J}) = S^{\iota a} \tag{4}$$

where $\omega^{\iota a}$ is the mass fraction of salt in the aqueous phase, $\mathbf{J}$ is the dispersive mass flux vector, and $S^{\iota a}$ is any salt source or sink in the aqueous phase. To close the conservation equation, Darcy's Law can again be utilized, and a Fickian dispersion equation can be used to describe the dispersive flux. The mass flux vector is mathematically described as:

$$\mathbf{J} = -\mathbf{D} \cdot \nabla C^{\iota a} \tag{5}$$

where $C^{\iota a}$ is the salt concentration (equal to $\omega^{\iota a} \rho^a$) and $\mathbf{D}$ is the dispersion tensor, defined in three dimensions by Bear [4] as:

$$\mathbf{D} = \mathbf{I}\, \alpha_T |\mathbf{q}| + (\alpha_L - \alpha_T) \frac{\mathbf{q}_i \mathbf{q}_j}{|\mathbf{q}|} + \epsilon^a D_m^{\iota a} \boldsymbol{\tau}_{ij} \qquad \text{for } i, j = 1, 2, 3 \tag{6}$$

Here, $D_m^{\iota a}$ is the free liquid diffusion coefficient of the salt species in the aqueous phase, α_L and α_T are the longitudinal and transverse dispersivities of the porous media, $\boldsymbol{\tau}_{ij}$ is the tortuosity tensor of the porous media, and $\mathbf{I}$ is the unit tensor. The dispersion process in SUTRA includes both diffusion and velocity-dependent dispersion. The tortuosity tensor can be accounted for by lowering the fluid diffusivity coefficient, which is a user defined parameter, as are the longitudinal and transverse dispersivities.

It should be noted here that the Fickian dispersion equation utilized in SUTRA may not be suitable for highly dense $CaBr_2$. In spite of the broad application of Fick's Law to describe salt flux, both experimental and theoretical analysis have shown that Fick's Law fails to accurately describe salt mass flux in systems with large concentration gradients [22]. A non-linear dispersion model has been proposed by Hassanizadeh to represent salt flux in high-concentration-gradient flow such as that seen in BBRT. This model is given as:

$$(1 + \beta|J|)\mathbf{J} = -\rho^a \mathbf{D} \cdot \nabla \omega^{ia} \tag{7}$$

where $\mathbf{D}$ is the same dispersion tensor appearing in Fick's Law, and β is a new dispersion parameter.

In order to close the set of flow and transport equations, constitutive relations must be employed for the aqueous phase density and viscosity. The density of a system is dependent on the temperature, pressure, solute concentration and fluid compressibility, and the viscosity of a system is dependent on temperature and solute concentration. However, fluid density has been seen to be a weak function of pressure and to depend primarily on fluid solute concentration and temperature. SUTRA solute transport simulations assume a constant temperature and employ a first order Taylor series expansion in concentration about a base density for the density model. This is given as:

$$\rho^a = \rho_0^a + \frac{\partial \rho^a}{\partial \omega^{\iota a}} \left(\omega^{\iota a} - \omega_0\right) \tag{8}$$

where ρ_0^a is a base density, or the density of freshwater, ω_0 is a base concentration, and $\omega^{\iota a}$ is the

solute concentration in the aqueous phase.

In addition, viscosity is said to be a weak function of pressure and to depend primarily on temperature. Viscosity has been shown to be dependent on solute concentration only in systems of high concentration. SUTRA solute transport simulations assume a solute concentration too small to affect viscosity, and therefore viscosity is held constant. However, due to the high concentration of $CaBr_2$, and its non-linear relationship to salt mass fraction, changes were made to the SUTRA source code to account for viscosity and density differences. These modifications are detailed in §3.1.1.

With porosity, intrinsic permeability, molecular diffusion, and dispersivity parameters defined, and with equations of state for density and viscosity, the system of equations is closed for saturated conditions. However, for unsaturated flow, aqueous phase saturation is no longer equal to porosity, adding additional unknowns. The addition of a gas phase elicits the use of a multiphase extension to Darcy's Law to account for the conservation of momentum. This is given as:

$$\mathbf{q}^a = \epsilon^a \mathbf{v}^a = -\frac{k k_r^a}{\mu^a} \left(\nabla p^a - \rho^a \mathbf{g} \right) \tag{9}$$

where k_r^a is the relative permeability to flow for the aqueous phase. Where intrinsic permeability can be defined as the ease of fluid flow through saturated pore space, relative permeability is the fraction of the intrinsic permeability that remains in unsaturated conditions.

In order to close the set of conservation equations for fluid in the unsaturated zone, a set of pressure-saturation relations must be employed. SUTRA employs the commonly used van Genuchten pressure-saturation equations:

$$k_r^a = \left(\frac{S_w - S_{wres}}{1 - S_{wres}} \right)^{\frac{1}{2}} \cdot \left\{ 1 - \left[1 - \left(\frac{S_w - S_{wres}}{1 - S_{wres}} \right)^{\frac{n}{n-1}} \right]^{\frac{n-1}{n}} \right\}^2 \tag{10a}$$

and

$$S_w = S_{wres} + (1 - S_{wres}) \left[\frac{1}{1 + (\alpha p_c)^n} \right]^{\frac{n-1}{n}} \tag{10b}$$

where S_w is the saturation of the aqueous phase (volume of aqueous phase per volume of pore space), S_{wres} is the residual saturation of the aqueous phase (the saturation below which the aqueous phase is not expected to fall), p_c is capillary pressure, and both α and n are parameters dependent upon the porous media [62]. Note that when conditions are saturated (p_c =0), k_r^a is equal to 1, and classical Darcy's law applies.

A list of parameters used for the simulations in this analysis can be found in §4.1.3 (Table 4.3). Section 3.2 details the application used to generate heterogeneous permeability fields for use in SUTRA and the methodology behind this application.

3.1.1 SUTRA Modifications

To facilitate this study, a few changes were made to the SUTRA source code. The modifications were useful in the representation of brine recovery and necessary for accurate representation of brine behavior.

Because the brine used at DNTS was both highly concentrated (0.53 salt mass fraction) and extremely dense, the SUTRA source code was modified to account for its viscosity and to accurately represent its density. A number of lab experiments using $CaBr_2$ were conducted to investigate the relationships between both salt mass fraction and density, and salt mass fraction and viscosity. The maximum variation in density in the experiments was that between freshwater (998.2 kg m^{-3}) and $CaBr_2$ (1700 kg m^{-3}). The viscosity ranged from 0.00097 kg m^{-1} s^{-1} (freshwater) to 0.006 kg m^{-1} s^{-1} ($CaBr_2$). Using a polynomial least-squares fitting method on data acquired from experiments, the following relations were derived:

$$\rho^a = \rho^a\left(\omega^{\iota a}\right) = 1127.69\left(\omega^{\iota a}\right)^2 + 736.01\omega^{\iota a} + 998.2 \tag{11a}$$

$$\mu^a = \mu^a\left(\omega^{\iota a}\right) = e^{\left[17.5\left(\omega^{\iota a}\right)^3 - 6.57\left(\omega^{\iota a}\right)^2 + 1.95\omega^{\iota a} - 6.94\right]} \tag{11b}$$

Figure 3.1 shows superpositions of both equations of state and the data points from which they were approximated. As can be seen, in the salt mass fraction range (0.0 kg kg^{-1} to 0.53 kg

kg^{-1}) for which density and viscosity were measured, the data and mathematical equations are in close agreement. The R^2 value for the density relationship is 0.9998, based on 6 data points, and the R^2 value for the viscosity function is 0.9973, based on 35 data points. The functions were added to the SUTRA source code so that the viscosity and density would be properly accounted for in the conservation equations.

Recall however, $CaBr_2$ likely exhibits non-Fickian behavior when added to a freshwater system, due to the ensuing high concentration gradient. Hassanizadeh and Leijnse have suggested that the use of a linear model for the dispersive mass flux, as implemented in SUTRA, inadequately predicts the dispersion of a system [22]. In a laboratory investigation, they observed the dispersive mass flux in high-concentration-gradient experiments (with differences as high as 0.23 kg kg^{-1}) to be two orders of magnitude greater than in low concentration gradient experiments with differences of 0.0015 kg kg^{-1}. However, to predict the higher flux in the high-concentration-gradient experiments, the value of longitudinal dispersivity had to be decreased by a factor of three. Though no dispersion studies involving fluid concentrations comparable to $CaBr_2$ are reported in the literature, it is likely that the use of a linear dispersion equation decreased the accuracy of simulations.

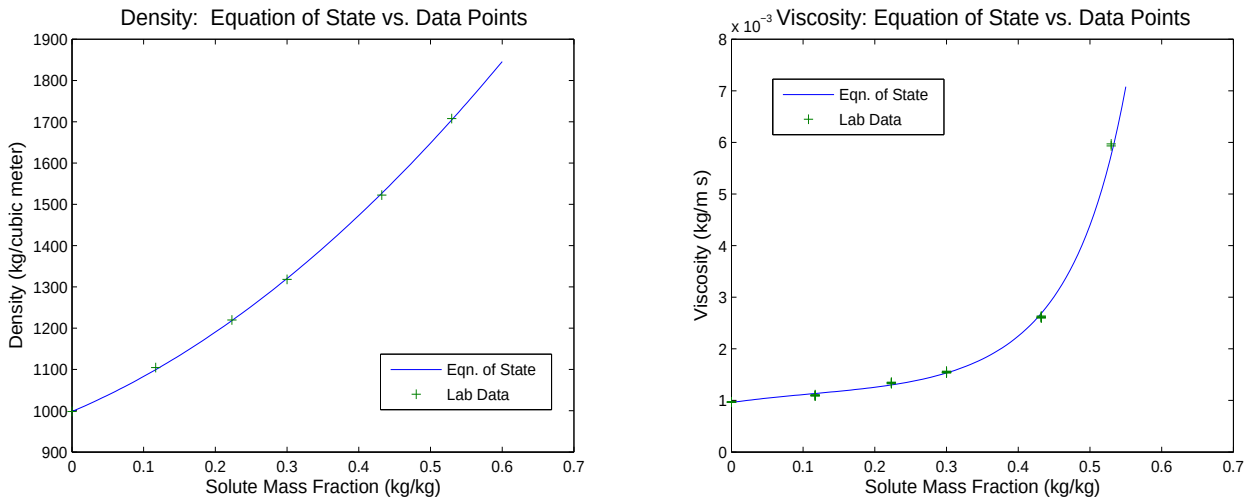

Figure 3.1: Density and viscosity as a function of salt mass fraction for calcium bromide

A further modification to the SUTRA source code involved altering extraction specifications and was essential for the brine recovery simulations. The SUTRA model requires mass rate inputs for any external sources or sinks. However, in a field-scale demonstration of BBRT, volumetric injection and extraction rates will be used in order to monitor the level of the water table in the aquifer. Since the amount of mass being recovered from a well varies with time, it is not feasible to convert a desired volume extraction rate to a mass rate necessary for SUTRA input.

Source code modifications were made such that a volume extraction rate could be specified in a simulation. To make this change, the concentration output at each time step in SUTRA, $(\omega^{\iota a})^t$, and the density equation of state reported previously, $\rho^a(\omega^{\iota a})$, were utilized. From a given volumetric extraction rate (E_V), the mass extraction rate at time step t (E_m^t), required by SUTRA, was approximated by:

$$E_m^t = E_V \cdot \left(\rho^a(\omega^{\iota a})^{t-1}\right) \tag{12}$$

With a small time step, Equation (12) gives a good approximation for the desired mass extraction rate at each time t. This change is advantageous for modeling the pilot study of BBRT, and it also allows for the use of a small unsaturated zone in simulations, as the amount of fluid in the system can be simulated to remain approximately constant.

3.1.2 Model Verification

SUTRA is a well-accepted and commonly used groundwater flow and transport model, and the documentation provides illustrations of its validity. Benchmark problems of variable-density flow are detailed, and model results are shown to be consistent with solutions known to be true. However, modifications made to the SUTRA source code elicited additional verification. In addition, preliminary comparisons between DNTS data and simulation data were made, to gain some understanding of the accuracy represented in the present study. These results are detailed in §5.1.

No well-studied problems of high viscosity and high density exist, and so preliminary simula-

tions were conducted to use for comparison. Since the original SUTRA code has been extensively tested and provides mass balance results with each simulation, it was assumed that the model presented accurate solutions to the preliminary variable-density brine transport problems. After the new viscosity and density functions were added, simulations were repeated, and the results were then compared to the preliminary simulations. Although the concentration profiles changed, as was to be expected, the mass balance results were equivalent.

The second change to SUTRA, the addition of a volume extraction option, had no impact on the precision of the results, as it simply varied the extraction rate at each time step. However, measures were taken to ascertain whether a given volume extraction rate did indeed result in an equivalent mass removal rate. To test the modification, various simulations were run with the injection and extraction of 13.25 m^3 of fluid over a number of different time periods. In each, the level of the water table was monitored over time. Because the water table elevation was seen to stay approximately constant in the simulations, it was concluded that an equal volume of fluid was being injected and extracted. Therefore, the goal of the modification was attained.

3.2 GSLIB Software Library

Application-based engineers initiated the study of geostatistics in the late 1960's. Originally, geostatistic research involved mapping of spatial distributions and the determination of a covariance model. Since this time, applications have been extended to include approximating uncertainty models based on the spatial distribution of data acquired. GSLIB, a geostatistical library developed by a Stanford research group, is a public-domain software package that includes many algorithms useful for geostatistical applications . The GSLIB source code utilized in this study was acquired with the second edition of GSLIB: Geostatistical Software Library and User's Guide, published in 1992 [9].

Correlated random permeability fields used in all heterogeneous simulations were created using the sequential Gaussian simulation (SGSIM) program provided by GSLIB. SGSIM creates

equi-probable realizations of data with a mean of 0 and variance of 1, with a given covariance structure, horizontal and vertical correlation lengths, and anisotropy factor. The data generated can thereafter be transformed by the user to a desired mean and variance.

The three most common covariance models used in groundwater modeling are Gaussian, exponential, and spherical, and they are shown in Figure 3.2. Represented here, each model is a function of separation distance only, which implies that each assumes stationarity, or a covariance independent of spatial location. The same covariance models can be used for non-stationary systems by techniques such as specifying a model and a parameter at a point in space. Traditionally, however, the stationary forms of the models are most commonly used.

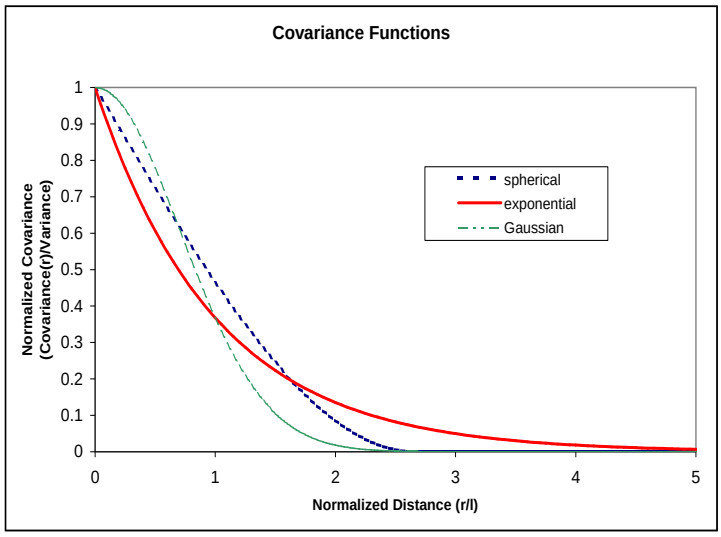

Figure 3.2: Spatial correlation models

The spatial distribution of a variable, Z, modeled by the Gaussian covariance function, is described by the following equation:

$$C_Z(\mathbf{r}) = \sigma_Z^2 \exp(-h^2) \tag{13}$$

where

$$h = \left| \sqrt{\sum_{i=1}^{m} \left(\frac{r_i}{l_i} \right)^2} \right|$$

and $\mathbf{r}$ = a separation vector between two points, σ_Z^2 = the variance of Z, m = the number of dimensions, and l_i = a scaling length parameter in the i^{th} dimension. The scaling length

parameter in a Gaussian model is equal to $2\lambda_i/\sqrt{\pi}$ where λ_i is referred to as the correlation length scale in the i^{th} direction. The correlation length scale represents the average length over which a variable is positively correlated at neighboring points [58]. When the Gaussian covariance function is used, the variable Z will be normally distributed, i.e., the probability density function (PDF) will be Gaussian. Note that the Gaussian covariance function is both continuous and differentiable at the origin (at zero separation distance), which implies a smooth transition of the variable between closely situated nodes. Therefore, this model, which creates visually continuous fields, is best used for gradually changing subsurface properties [50].

The exponential covariance model is written as:

$$C_Z(\mathbf{r}) = \sigma_Z^2 \exp(-h) \tag{14}$$

The scaling length parameter in this model is equal to the correlation length scale ($l_i = \lambda_i$). The exponential model is best suited for a rugged subsurface in which porous media properties might vary greatly. This can be implied from the function's shape, which is nondifferentiable at the origin. In this case, the model is a better fit for modeling of larger domains, as sharp transitions occur between neighboring nodes. Also, the spatial correlation decreases more rapidly than in both the Gaussian and spherical models [50].

The spherical covariance function is most closely related to the exponential function and is suitable for similar types of domains. The spherical covariance function is given as:

$$C_Z(\mathbf{r}) = \begin{cases} \sigma_Z^2 \left[1 - 3h/2 + h^3/2\right], & h \leq 1 \\ 0 \quad \text{otherwise} \end{cases} \tag{15}$$

Its most distinctive difference from the exponential covariance function is that the correlation is equal to zero at a finite separation distance determined by the scaling length parameter. The scaling length parameter, l_i, in the spherical model is equal to $8\lambda_i/3$.

In addition to the previous covariance functions, a model referred to as a "nugget model" may be useful, especially in the quantification of a domain which has no correlation over the grid chosen. This function may be employed if the distance between nodes in a numerical simulation

is larger than the correlation length, in which case there is assumed to be no correlation between any of the nodes [50]. Among the covariance functions detailed, a model of a variable comes close to being represented by a nugget model, or having "zero nugget," as the correlation length tends to zero. The nugget covariance function is equal to the variance at zero separation distance and rapidly descends to zero covariance thereafter.

Overall, stochastic methods are able to account for many aspects of spatial variability. Representing anisotropic systems, or systems whose covariance varies with a rotation of the domain, is accomplished by differences in correlation length scales of each dimension. The nugget determines the small scale spatial variability, as a higher nugget produces a lower proportion of correlated residuals, resulting in a smoother distribution. The covariance structure chosen affects the large-scale variability, and the probability distribution function determines the mean, variance and frequency of a variable. Lastly, varying the correlation length scale results in different sizes of continuous images [50]. The flexibility and possibilities afforded by these methods make them popular for heterogeneity representation in groundwater modeling.

3.3 Computing Environment

The modified SUTRA source code was compiled using the IBM xlf90 Fortran 90 compiler. Compilation was performed on the University of North Carolina's IBM AIX login node, Happy. SUTRA simulations were submitted to and executed on the University's processor high-performance computing server, Yatta, a 32-CPU IBM P690. Windows executable files available for SutraPlot and SutraPrep were downloaded from
http://water.usgs.gov/nrp/gwsoftware/sutra.html. These were run on a Windows PC for pre-processing and post-processing uses.

GSLIB source code was compiled on the University of North Carolina's 352-CPU Linux Beowulf cluster, Baobab, using f77 Fortran 77 compiler. The SGSIM executable was also run on Baobab, a sealed server managed by Information Technology Services for scientific computing

and available to the research community on campus.

3.4 Analysis

Three types of simulations were performed using the GSLIB software and SUTRA model detailed previously. The methods of analyzing the simulation results are detailed in the following sections.

3.4.1 Brine Emplacement

The first stage of BBRT involves the establishment of a layer of dense brine below a DNAPL source zone. The high viscosity of brines used in the remediation process causes mounding around injection wells, which results in large density differences at a given elevation across the domain. This phenomenon was observed in three-dimensional laboratory experiments using $CaBr_2$ to form a brine barrier. At later times, these mounds were seen to dissipate, and the density within the system became more stratified. Therefore, an increase in brine mounding results in a longer time scale to establish a stratified brine barrier.

Because dense brines are expensive and remediation experiments are timely, approximating the most efficient means of creating a brine barrier is important. This involves approximating a brine injection rate that will minimize mounding yet advance the emplacement of brine in an efficient manner. In addition to injection rate, the degree of heterogeneity in the subsurface will also affect the amount of mounding that will occur in the system.

Brine emplacement simulations representative of the process as it occurred at DNTS were conducted in this study. Breakthrough curves of solute concentration, across the domain, at a constant depth were compared to analyze the amount of brine mounding that occurs for a given injection rate and heterogeneity profile. The mean and variance of the concentration at different depths were evaluated to determine the change in thickness of a dense layer over time. In addition, the simulations were analyzed to detect if any types of heterogeneity led to instabilities, or less dense fluid lying below a denser fluid. Concentration plots were also generated to visualize

the mounding that occurs in a dense brine system.

Model results can determine the approximate length of time required to reach a desired concentration with a tolerated amount of mounding in the system. This information can assist in decision-making during field-scale implementations of BBRT and help predict a range of times that may be expected to complete the emplacement process.

3.4.2 Brine Recovery

As an optimal brine injection strategy is essential to remediate areas in a timely manner, efficient recovery of brine thereafter is equally important. Dense brines used in BBRT are expensive, and therefore their reuse is beneficial. After brine is removed from the system, it can be reconcentrated for later use by evaporation. The cost of this process decreases as the concentration of the brine increases, and therefore the cost of recycling brine is a function of the solute concentration as it is extracted from the system. For this reason, it is important to have a knowledge of fluid concentrations that will be extracted throughout the brine recovery procedure.

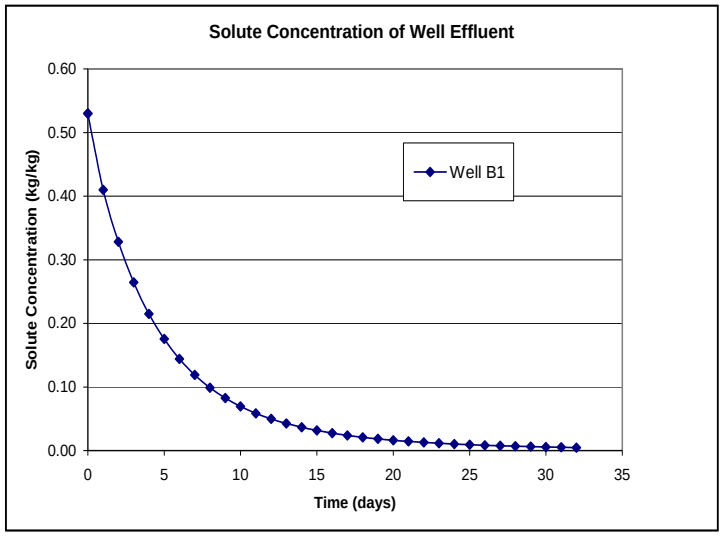

Figure 3.3: Typical profile of solute concentration in fluid effluent during brine recovery process

Figure 3.3 represents a typical profile of solute concentrations extracted from a well during the brine recovery process. Because the extraction rates vary with the simulations conducted in

this analysis, the integration of concentration curves could not be compared to analyze the total mass recovered. Therefore, mass fractions provided by SUTRA were converted to a corresponding density. This density, in addition to the volume extraction rate used, gives a total mass rate extracted at each time step reported. Numerical integration of the area under this curve, which is an approximation of the total mass recovered, was compared among simulations.

During brine extraction, freshwater in simultaneously injected into the domain to maintain a certain water level and to further induce flow. Two methods of freshwater flushing were compared among simulations. The fraction of mass removed as a function of pore volume of fluid extracted was analyzed to determine the efficiency of an extraction rate for a specific heterogeneous field and flushing scenario. Comparisons were made to determine both the impacts of heterogeneity and the effects of varying pumping rates on brine recovery efficiency. Simulation results can be used to determine efficient brine recovery rates, to predict the time required to recover the solute mass desired and to compare the cost of brine reconcentration between different recovery scenarios.

3.4.3 Viscous Effects of Brine

To evaluate the dominant mechanisms for brine behavior, simulations were conducted in which brine properties were manipulated. It was assumed that, by separating these properties, the effects of their independent forces could be approximated. Identical simulations were performed, each with one of three different fluids:

1. a dense, yet non-viscous brine,
2. a viscous, yet non-dense brine, or
3. a dense and viscous brine.

Average velocities across the domain were observed to evaluate the differences in solute transport between simulations. Comparison of velocity values allowed for the approximation of

the effects of viscosity and density on phase flow. In addition, concentration profiles were plotted to investigate whether instabilities formed in the simulations.

4 Application

Three groups of simulations were conducted to evaluate the behavior of brine in the subsurface. The first two groups—modeling brine emplacement and brine recovery—were based on a pilot study at DNTS, though they were generalized to apply to typical BBRT implementation and to allow for a more thorough investigation of the processes involved. The third group of simulations utilized a regular rectangular domain to investigate the effects of viscosity and density on brine flow and transport. The simulations in this analysis represent grid independent solutions as evidenced by an evaluation of the L^1- and L^2-norms of simulated concentration values. A detailed summary of the simulations is provided in the following sections.

4.1 Brine Emplacement

The allocation of injection and extraction wells used for brine emplacement at DNTS was determined based on the location of each well and its corresponding depth to an impermeable clay layer. With no information on the heterogeneity of the domain, it was assumed that depth of the domain was the most important variable in the decision-making process. As an irregularly shaped clay layer was used on which to form the brine barrier, the deepest points of the clay layer, requiring the greatest volume to fill, were chosen as initial injection locations. Holding the DNTS pumping strategy constant, three-dimensional simulations were conducted to determine the effects of heterogeneity, combined with varying injection rates, on brine emplacement.

4.1.1 Dover National Test Site Domain

A plan view of the Dover National Test Site test cell, which is approximately 4.8 meters $\times$ 3.2 meters, is shown in Figure 4.1. The cell is surrounded by double sheet piling, which has

been inserted into the ground and through a clay layer at an average depth of approximately 12.2 meters. The clay layer, which was used for the formation of the brine barrier, is irregularly shaped, adding complications to both the physical experiment and to computer modeling.

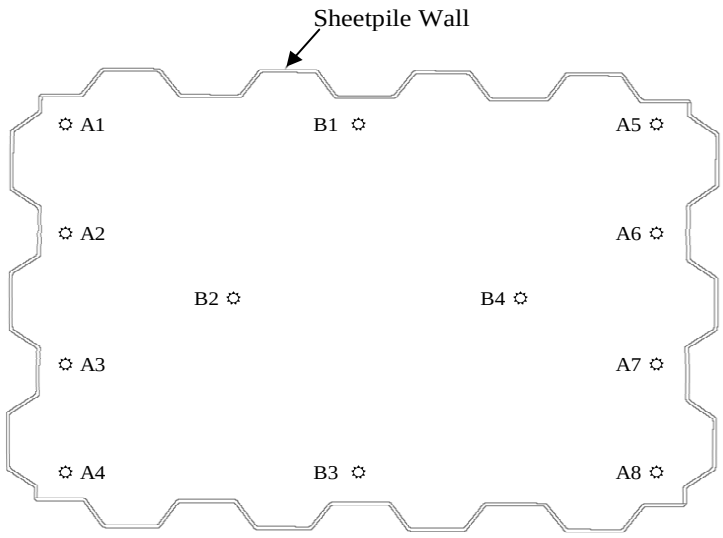

Figure 4.1: Plan view of DNTS test cell with injection and extraction wells labeled

Data, which can be found in Table 4.1, has been collected on the depth to the clay layer at each of the well locations seen in Figure 4.1 [49]. In order to construct a mesh to represent the DNTS test cell in SUTRA, a Matlab script was written to create an irregularly shaped domain. The code used data from Table 4.1 to approximate the clay surface throughout the system using triangle-based linear interpolation and to output a desired discretized domain suitable for a SUTRA input file. A three-dimensional image of the interpolated clay layer, which represented a Neumann boundary condition equal to zero in the simulations, is shown in Figure 4.2.

The generated discretized domain spanned [0,4.8] meters along the x axis and [0,3.2] meters along the y axis. The maximum z axis value was set to 9.0 meters below ground level (z = -9.0 meters) and decreased to the clay layer below. The domain was discretized into 41 elements along the x axis, 28 elements along the y axis and 46 elements along the z axis. Realizations of permeability data were generated using SGSIM for a three-dimensional domain specific to DNTS. It was assumed that changes in subsurface properties were gradual and that the domain was best

Table 4.1: Depth to clay at injection and extraction well locations

Well No.	Depth (m)		Well No.	Depth (m)
A1	12.10		A7	11.73
A2	12.37		A8	12.01
A3	12.19		B1	12.50
A4	12.34		B2	12.53
A5	12.41		B3	12.50
A6	12.31		B4	12.25

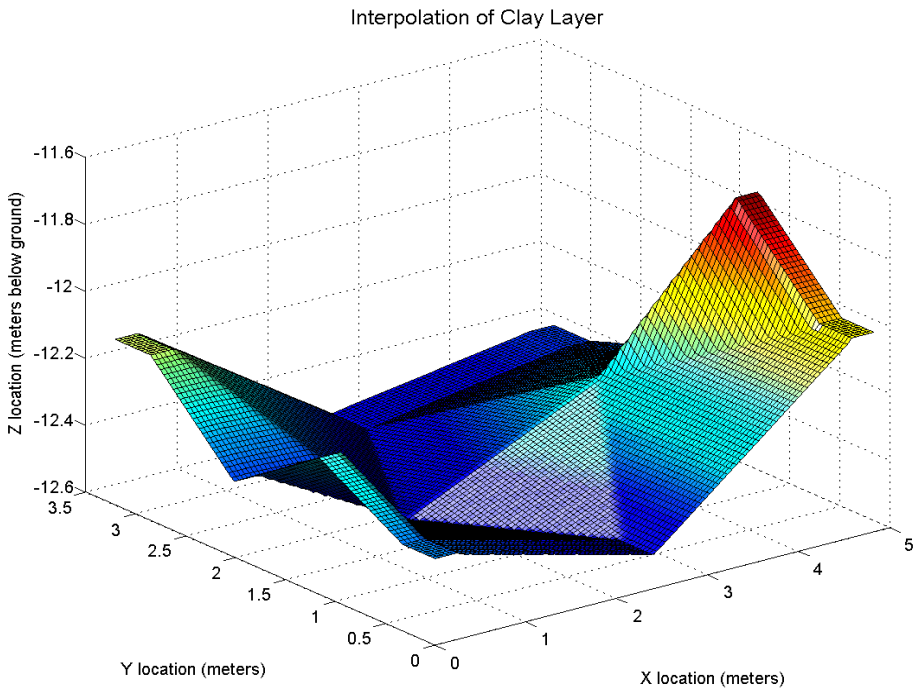

Figure 4.2: Interpolated clay layer at DNTS based on 12 data points

represented by a Gaussian covariance model. Due to a lack of spatial hydraulic conductivity data, a correlation length scale could not be determined. Values of 0.5 m and 2.5 m for the vertical and horizontal correlation length scales, respectively, were assumed, and the domain was considered isotropic. The data realizations were transformed to a set with a mean value of ln

3×10^{-12} m^2, where 3×10^{-12} m^2 was the one value of intrinsic permeability available for the test cell [49]. A range of variances were considered to analyze the disparities this could create.

SGSIM was employed to create sets of data both for heterogeneous domains represented by a Gaussian SRF and for layered domains. In the latter, SGSIM was used to indicate a desired vertical correlation length scale and vertical covariance structure. Detailed information on permeability fields used in each brine emplacement simulation can be seen in Table 4.2 in Section 4.1.3.

4.1.2 Boundary and Initial Conditions

Initial pressure conditions were hydrostatic with pressure equal to zero at z = -10.0 meters. This allowed for the representation of an unsaturated zone from z = [-10.0,-9.0] meters, to more realistically depict the brine emplacement process at DNTS. Initial groundwater concentration was zero throughout the domain. All boundaries were Neumann boundaries equal to zero, allowing no dispersive flux normal to the boundaries.

4.1.3 Simulation Summary

Each brine emplacement simulation involved the injection of 13.25 m^3 of brine, through various injection wells, across the bottom 0.6 meters of each well. Initially, half this volume was injected in wells B1, B2, B3, and B4. Concurrently, an equivalent volume was extracted from the upper portion of the saturated zone through wells A1, A2, A3, A4, A5, A6, and A8 (well A7 was inoperable throughout the field experiment and, so, was removed from simulations). Thereafter, the injection and extraction wells were reversed, and the remaining 6.625 m^3 of brine was injected.

Variable in the simulations were pumping rate, total pumping time, and permeability fields. A summary of values for each simulation is found in Table 4.2. A list of model parameters used in all brine emplacement and recovery simulations can be found in Table 4.3.

Table 4.2: Summary of brine emplacement simulations

Simulation	Domain	Variance	λ_x	λ_z	Days	m^3 Day^{-1}
E1	Homogeneous	0	-	-	32	0.414
E2	Gaussian SRF	0.25	2.5 m	0.5 m	32	0.414
E3	Gaussian SRF	1	2.5 m	0.5 m	32	0.414
E4	Layered	0.25	-	0.5 m	32	0.414
E5	Layered	1	-	0.5 m	32	0.414
E6	Layered	2	-	0.5 m	32	0.414
E7	Homogeneous	0	-	-	12	1.104
E8	Gaussian SRF	0.25	2.5 m	0.5 m	12	1.104
E9	Gaussian SRF	1	2.5 m	0.5 m	12	1.104
E10	Layered	0.25	-	0.5 m	12	1.104
E11	Layered	1	-	0.5 m	12	1.104
E12	Layered	2	-	0.5 m	12	1.104

Table 4.3: Model parameters used in brine emplacement and recovery simulations

Model parameter	Value
Freshwater density	998.2 kg m^{-3}
Freshwater viscosity	9.683×10^{-4} kg m^{-1} s^{-1}
Brine source concentration	0.53 kg kg^{-1}
Brine source density	1700 kg m^{-3}
Brine source viscosity	6.0×10^{-6} kg m^{-1} s^{-1}
Water compressibility	0.0 m s^2 kg^{-1}
Soil compressibility	0.0 m s^2 kg^{-1}
Porosity	0.35
Mean intrinsic permeability	3×10^{-12} m^2
Longitudinal dispersivity	0.48 m
Transverse dispersivity	0.16 m
Molecular diffusivity	1.22×10^{-9} m^2 s^{-1}
Acceleration due to gravity	9.8 m s^{-2}
Aquifer length	4.8 m
Aquifer width	3.2 m
n (van Genuchten)	2.0
α (van Genuchten)	5×10^{-5} m^{-1}

4.2 Brine Recovery

The brine recovery process involves both the extraction of fluid from the bottom of the domain and the injection of an equal volume of freshwater at auxiliary locations. This combination both maintains the water table elevation and creates a stronger gradient for flow toward extraction wells. Though it is optimal for brine to be extracted in a timely manner, increasing rates of freshwater flushing can lead to brine instabilities, which ultimately make extraction less efficient. These instabilities, as described previously, are also affected by subsurface heterogeneity. Simulations with varying extraction rates and degrees of heterogeneity were conducted to analyze the total mass removed from the system.

4.2.1 Model Domain, Boundary Conditions and Initial Conditions

Since the water table was lower prior to the brine recovery phase than it was prior to brine emplacement during the field experiment, the initial conditions were altered for the recovery simulations. A pressure of zero was set at z = -11.5 meters, thus creating saturated conditions below this level. Initial groundwater concentration was represented by fully concentrated brine between the clay surface and z = -11.5 meters, with a brine layer of linearly decreasing concentration between z = -11.5 meters and z = -10.9 meters. All boundaries were Neumann boundaries equal to zero. The same model domain and discretization were used in the brine recovery simulations as were used for brine emplacement.

4.2.2 Simulation Summary

Two types of brine recovery simulations were conducted—those in which freshwater was injected along the bottom 0.3 meters of the domain during extraction and those in which freshwater was injected along the upper 0.3 meters of the saturated zone during extraction. In each simulation, a total of 13.25 m^3 of fluid was extracted from wells B1, B2, B3 and B4, and freshwater was simultaneously injected into wells A1, A2, A3, A4, A5, A6,and A8. A summary of the recovery simulations conducted, which utilized the same parameters found in Table 4.3, can be

seen in Table 4.4.

Table 4.4: Summary of brine recovery simulations

Simulation	Domain	Variance	λ_x	λ_z	Days	m^3 Day^{-1}	Flush Location
R17	Homogeneous	0	-	-	12	1.104	Clay Layer
R18	Gaussian SRF	0.25	2.5 m	0.5 m	12	1.104	Clay Layer
R19	Layered	0.25	2.5 m	0.5 m	12	1.104	Clay Layer
R20	Layered	1	-	0.5 m	12	1.104	Clay Layer
R21	Homogeneous	0	-	-	12	1.104	Water Table
R22	Gaussian SRF	0.25	2.5 m	0.5 m	12	1.104	Water Table
R23	Layered	0.25	2.5 m	0.5 m	12	1.104	Water Table
R24	Layered	1	-	0.5 m	12	1.104	Water Table

Table 4.4: Summary of brine recovery simulations
*Continued on following page

Simulation	Domain	Variance	λ_x	λ_z	Days	m^3 Day^{-1}	Flush Location
R1	Homogeneous	0	-	-	32	0.414	Clay Layer
R2	Gaussian SRF	0.25	2.5 m	0.5 m	32	0.414	Clay Layer
R3	Layered	0.25	2.5 m	0.5 m	32	0.414	Clay Layer
R4	Layered	1	-	0 .5 m	32	0.414	Clay Layer
R5	Homogeneous	0	-	-	32	0.414	Water Table
R6	Gaussian SRF	0.25	2.5 m	0.5 m	32	0.414	Water Table
R7	Layered	0.25	2.5 m	0.5 m	32	0.414	Water Table
R8	Layered	1	-	0.5 m	32	0.414	Water Table
R9	Homogeneous	0	-	-	18	0.736	Clay Layer
R10	Gaussian SRF	0.25	2.5 m	0.5 m	18	0.736	Clay Layer
R11	Layered	0.25	2.5 m	0.5 m	18	0.736	Clay Layer
R12	Layered	1	-	0.5 m	18	0.736	Clay Layer
R13	Homogeneous	0	-	-	18	0.736	Water Table
R14	Gaussian SRF	0.25	2.5 m	0.5 m	18	0.736	Water Table
R15	Layered	0.25	2.5 m	0.5 m	18	0.736	Water Table
R16	Layered	1	-	0.5 m	18	0.736	Water Table

4.3 Viscosity Simulations

A group of simulations was conducted to evaluate the effects of viscosity on brine flow and transport in a confined aquifer. Since SUTRA neglects viscosity variations, as do most groundwater flow and transport models, the goal of this investigation was to assess the impact this negligence has on the flow of a fluid representative of $CaBr_2$. This evaluation was possible because of modifications made in the SUTRA source code.

The simulations were divided into Set 1 simulations (W1—W6) and Set 2 simulations (B1—B6). Set 1 corresponds to a freshwater-saturated system that is displaced by brine flowing from a vertical boundary. Set 2 corresponds to a saturated system of initial concentration 0.53 kg kg^{-1} that is displaced by freshwater from the maximum horizontal boundary. The combination of simulations was intended to compare the differences in pattern formation between systems in which:

1. a dense, non-viscous fluid displaces freshwater (W1/W4),
2. a viscous, non-dense fluid displaces freshwater (W2/W5),
3. a dense, viscous fluid displaces freshwater (W3/W6),
4. freshwater displaces a dense, non-viscous fluid (B1/B4),
5. freshwater displaces a viscous, non-dense fluid (B2/B5), and
6. freshwater displaces a dense, viscous fluid (B3/B6).

Comparison allows for the investigation of independent viscous effects as well as the effects of high viscosity in combination with high density. Both a homogeneous and a heterogeneous simulation were performed for each case.

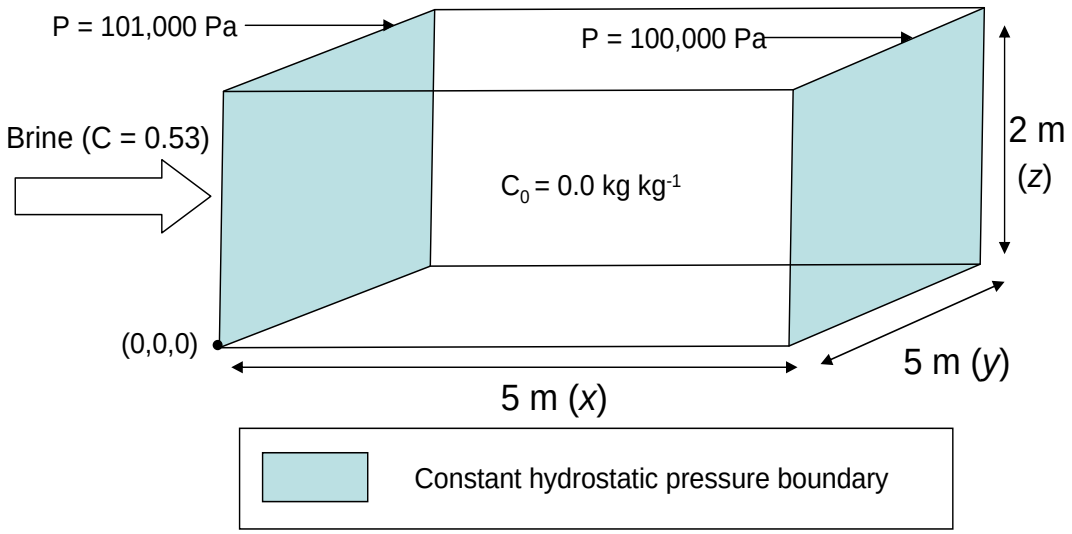

Figure 4.3: Model domain, boundary conditions and initial conditions for simulations W1—W6

4.3.1 Model Domain, Boundary Conditions and Initial Conditions

The domain used in both Set 1 and Set 2 simulations was 5 meters in the x axis direction, 5 meters in the y axis direction and 2 meters in the z axis direction, discretized into 40 elements in each dimension. A representation of the scenario used in simulations W1—W6 is seen in Figure 4.3. Initial pressure in these simulations was hydrostatic, with pressure equal to 101,000 Pa on the top boundary, and initial groundwater concentration was zero. The $x = 0$ m boundary condition was hydrostatic with a value of 101,000 Pa at the maximum vertical boundary, and the $x = 5$ meter boundary condition was hydrostatic with a value of 100,000 Pa at the maximum vertical boundary. All other boundaries were Neumann boundaries equal to zero. The pressure gradient in the x-direction allowed fluid to flow into the domain from the $x = 0$ m plane. The concentration of inflowing fluid was specified as 0.53 kg kg^{-1}.

Simulations B1—B6 correspond to a system initially at hydrostatic pressure, with pressure equal to 101,000 Pa on the top boundary. All boundaries were Neumann boundaries equal to zero except the $x = 0$ meter and $x = 5$ meter planes, both of which had constant hydrostatic pressure conditions. The system was initially saturated with fluid of concentration 0.53 kg kg^{-1}, and freshwater was injected across the top of the domain as shown in Figure 4.4.

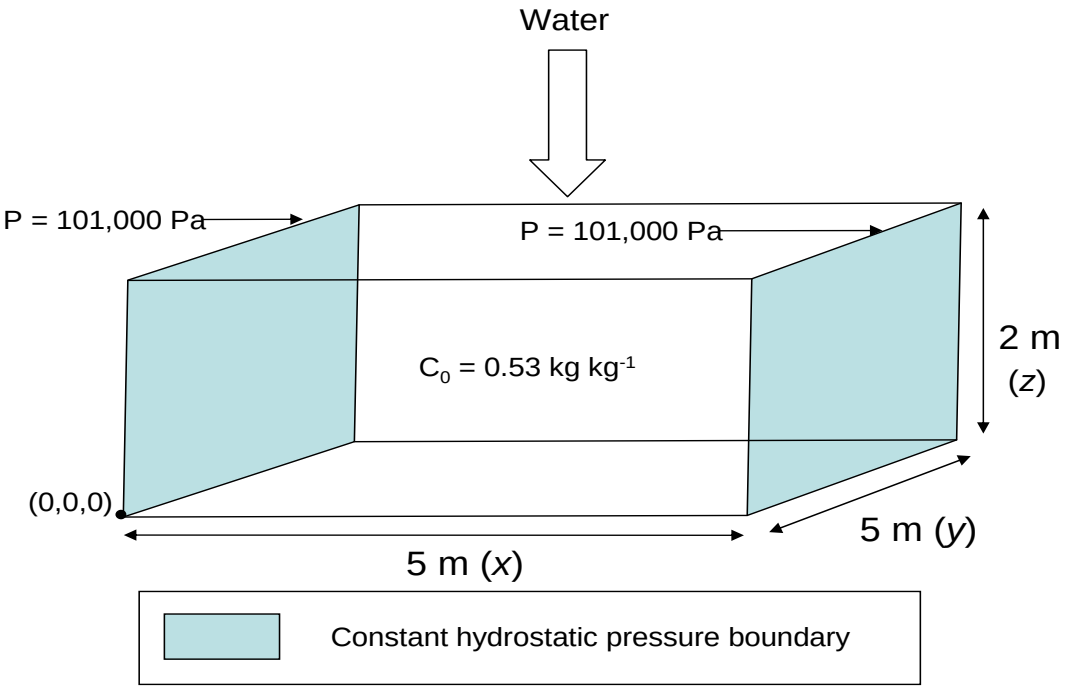

Figure 4.4: Model domain, boundary conditions and initial conditions for simulations B1—B6

4.3.2 Simulation Summary

Simulations W1—W6 involved the introduction of concentrated fluid, induced by a horizontal pressure gradient, into a freshwater-saturated domain. The gradient, which was held constant by the boundary conditions, was a decrease in 1,000 Pa across 5 horizontal meters, equivalent to a change in hydraulic head of 0.1 meters over 5 horizontal meters. The inflowing fluid concentration was 0.53 kg kg^{-1}. The simulation time was 2.5 days, and a 4 minute time step was used.

Simulations B1—B6 involved the displacement of a brine-saturated domain by freshwater injected across the maximum horizontal boundary. The fluid source was added at a rate of 72.62 cubic meters per day for 2.5 days. The time step used in the simulations was 4 minutes.

Tables are supplied to detail the simulations. Tables 4.5 and 4.6 provide information about the porous media type, the displacing and ambient fluids, and the brine properties that are accounted for in specific simulations. All homogeneous domains have an intrinsic permeability, k, equal to 3×10^{-12} m^2. All heterogeneous domains are distributed such that $Y \sim \mathrm{N}(ln$

Table 4.5: Summary of Set 1 viscosity simulations

Simulation	Domain	Displacing Fluid	Brine Properties
W1	Homogeneous	Brine	Dense
W2	Homogeneous	Brine	Viscous
W3	Homogeneous	Brine	Dense & Viscous
W4	Heterogeneous	Brine	Dense
W5	Heterogeneous	Brine	Viscous
W6	Heterogeneous	Brine	Dense & Viscous

3×10^{-12},1) where $k = e^{Y}$. The heterogeneous domains have a Gaussian covariance structure, where the horizontal correlation length scale is equal to 2.5 meters, and the vertical correlation length scale is equal to 0.5 meters. Tables 4.7—4.10 group the simulations into homogeneous and heterogeneous Set 1 simulations (in which freshwater is displaced by brine) and homogeneous and heterogeneous Set 2 simulations (in which brine is displaced by freshwater). The tables provide parameters used for the properties of freshwater and fully concentrated (0.53 kg kg^{-1}) fluid.

Table 4.6: Summary of Set 2 viscosity simulations

Simulation	Domain	Displacing Fluid	Brine Properties
B1	Homogeneous	Freshwater	Dense
B2	Homogeneous	Freshwater	Viscous
B3	Homogeneous	Freshwater	Dense & Viscous
B4	Heterogeneous	Freshwater	Dense
B5	Heterogeneous	Freshwater	Viscous
B6	Heterogeneous	Freshwater	Dense & Viscous

Table 4.7: Set 1: Homogeneous viscosity simulations

Simulation	Initial Density (kg m^{-3})	Initial Viscosity (kg m^{-1} s^{-1})	Displacing Fluid Density (kg m^{-3})	Displacing Fluid Viscosity (kg m^{-1} s^{-1})
W1	998.2	9.7×10^{-4}	1700.0	9.7×10^{-4}
W2	998.2	9.7×10^{-4}	998.2	6.0×10^{-3}
W3	998.2	9.7×10^{-4}	1700.0	6.0×10^{-3}

Table 4.8: Set 1: Heterogeneous viscosity simulations

Simulation	Initial Density (kg m^{-3})	Initial Viscosity (kg m^{-1} s^{-1})	Displacing Fluid Density (kg m^{-3})	Displacing Fluid Viscosity (kg m^{-1} s^{-1})
W4	998.2	9.7×10^{-4}	1700.0	9.7×10^{-4}
W5	998.2	9.7×10^{-4}	998.2	6.0×10^{-3}
W6	998.2	9.7×10^{-4}	1700.0	6.0×10^{-3}

Table 4.9: Set 2: Homogeneous viscosity simulations

Simulation	Initial Density (kg m^{-3})	Initial Viscosity (kg m^{-1} s^{-1})	Displacing Fluid Density (kg m^{-3})	Displacing Fluid Viscosity (kg m^{-1} s^{-1})
B1	1700.0	9.7×10^{-4}	998.2	9.7×10^{-4}
B2	998.2	6.0×10^{-3}	998.2	9.7×10^{-4}
B3	1700.0	6.0×10^{-3}	998.2	9.7×10^{-4}

Table 4.10: Set 2: Heterogeneous viscosity simulations

Simulation	Initial Density (kg m^{-3})	Initial Viscosity (kg m^{-1} s^{-1})	Displacing Fluid Density (kg m^{-3})	Displacing Fluid Viscosity (kg m^{-1} s^{-1})
B4	1700.0	9.7×10^{-4}	998.2	9.7×10^{-4}
B5	998.2	6.0×10^{-3}	998.2	9.7×10^{-4}
B6	1700.0	6.0×10^{-3}	998.2	9.7×10^{-4}

5 Results and Discussion

5.1 Brine Emplacement at Dover National Test Site

Homogeneous SUTRA simulations were conducted to represent brine emplacement as it occurred at DNTS. A total of 0.103 PV of brine was added to the domain using the same injection and extraction schematic detailed in the brine emplacement simulations. Figures 5.1(a)—5.1(d) demonstrate measured and simulated data at different multi-level sampler sites in the domain, and Figures 5.2(a) and 5.2(b) provide simulated and measured data after a 0.041 PV and 0.103 PV injection of brine.

This preliminary comparison showed model results to provide a good estimation of concentration variation throughout the domain, though instabilities observed in the field were not predicted, and simulated concentrations were consistently lower than data obtained. Though SUTRA concentration results were significantly less than actual data suggested, model predictions became better as more brine was added to the system. Note that the concentration data provided, which was much greater than simulated, was obtained from multi-level sampler locations, away from injection and extraction wells. Therefore, since an equivalent volume of mass was added to the system in simulations as was added in the field experiment, it is assumed that simulated data at injection well locations may be higher than measured. This could result from an underestimation of dispersion in the numerical model, heterogeneities in the field, measurement error, or simulation imprecision. However, to determine the validity of these assumptions, a more thorough investigation of data analysis must be made. Comparison of representative brine recovery simulations to measured data would also further demonstrate the accuracy of SUTRA for BBRT modeling.

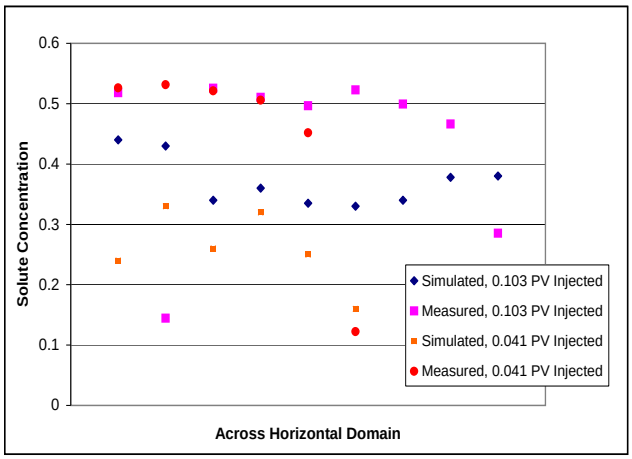

(a) Simulated and measured concentrations, 12 meters below ground surface

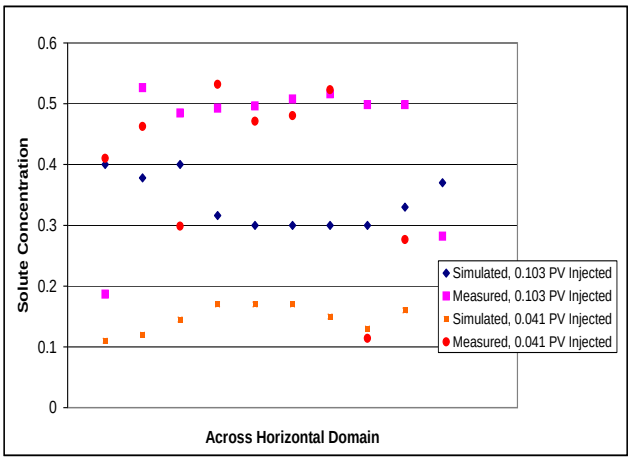

(b) Simulated and measured concentrations, 11.7 meters below ground surface

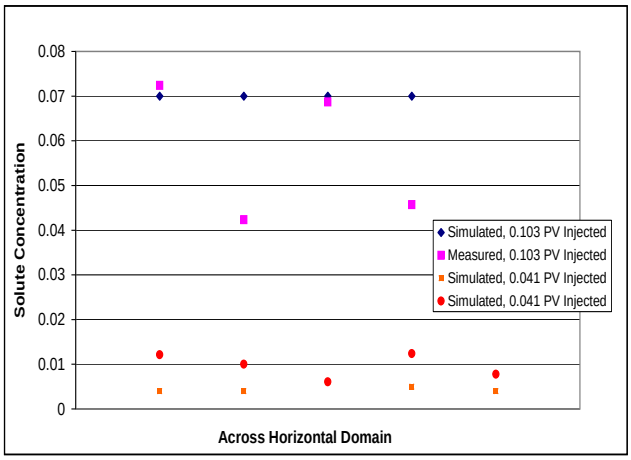

(c) Simulated and measured concentrations, 11.4 meters below ground surface

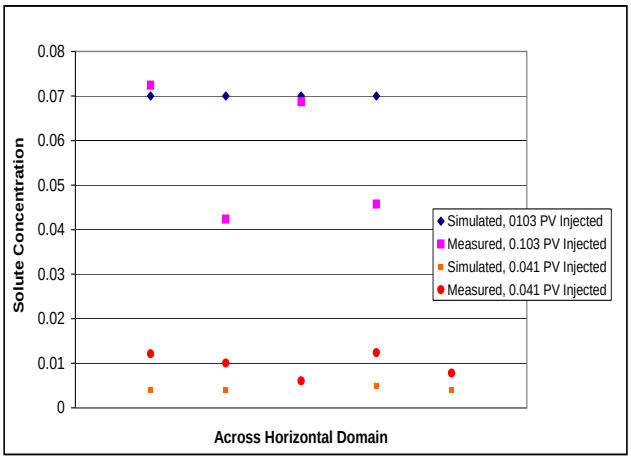

(d) Simulated and measured concentrations, 10.5 meters below ground surface

Figure 5.1: Simulated and measured concentrations at various multi-level sampler sites

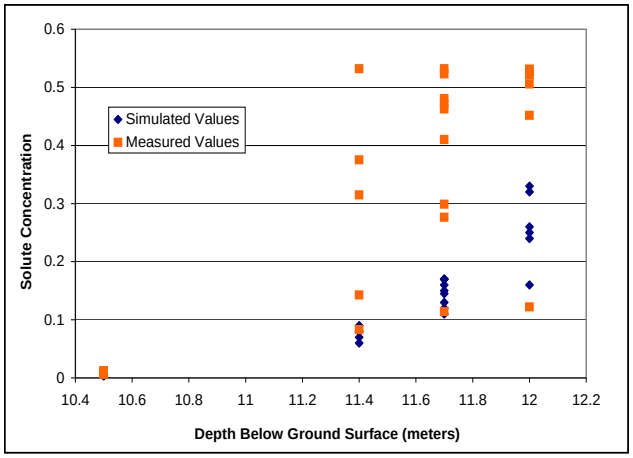

(a) Simulated and measured concentrations after 0.041 PV brine injected

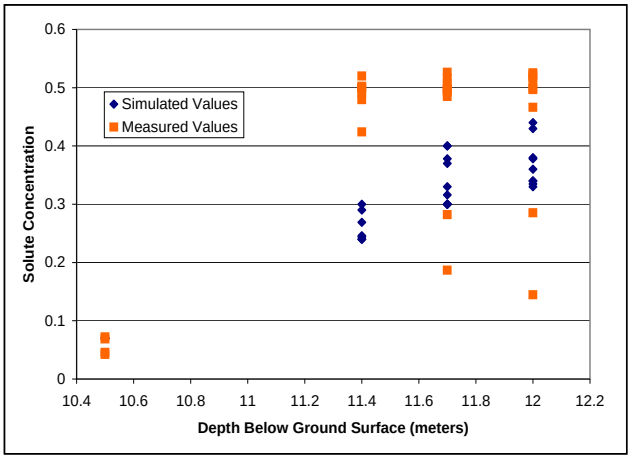

(b) Simulated and measured concentrations after 0.103 PV brine injected

Figure 5.2: Simulated and measured concentrations at two injection times

5.2 Brine Emplacement Simulations

The first group of simulations examined the effects of subsurface heterogeneity and injection rate variation on the brine emplacement process. The injection of 13.25 m^3, or 0.33 pore volume (PV), of brine across the lower 0.6 meters of injection wells was simulated. Solute concentration across the domain was monitored over time to evaluate the establishment and stratification of the brine layer. Initially, breakthrough curves (BTCs) were plotted at injection and extraction well locations, as well as at five other monitoring points. These points, labeled C1—C5 in Figure 5.3, were selected to compare concentration profiles at well locations to profiles at points between the wells.

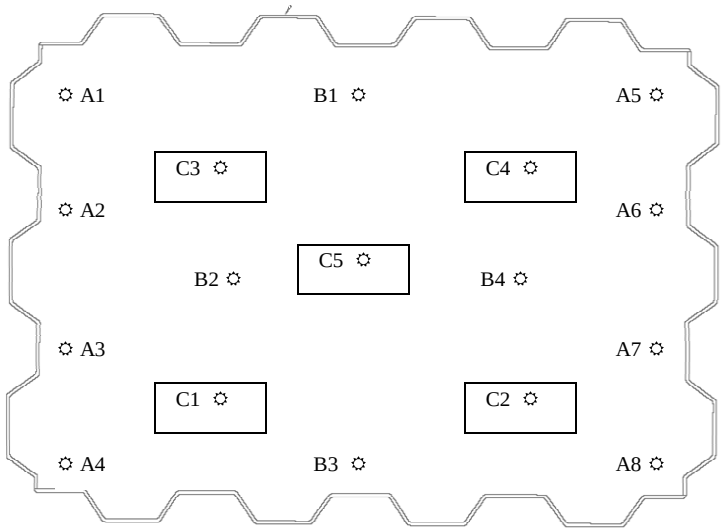

Figure 5.3: Plan view of DNTS test cell with monitoring points C1—C5 labeled

Analysis of BTCs demonstrated that the variance among constant elevation points monitored was not always indicative of the variance across the domain at that elevation. For example, it was observed in simulation E11 that at a height 0.6 meters above the clay layer (ACL) there was a large variance in concentration between the injection and extraction wells relative to that in other simulations. However, a small concentration variance relative to other simulations was seen between locations C1—C5. This supports the idea that average values across horizontal

planes must be used to make significant conclusions.

Nonetheless, example BTCs are given to demonstrate the differences between concentrations over time at well locations and at points in between. Figures 5.4(a)—5.4(d) represent BTC patterns typical of those seen in the 12 brine emplacement simulations. Figures 5.4(a) and 5.4(b) give BTCs from simulation E1 at a height 0.6 meters above the clay layer, while Figures 5.4(c) and 5.4(d) represent BTCs at the clay layer surface from simulation E11.

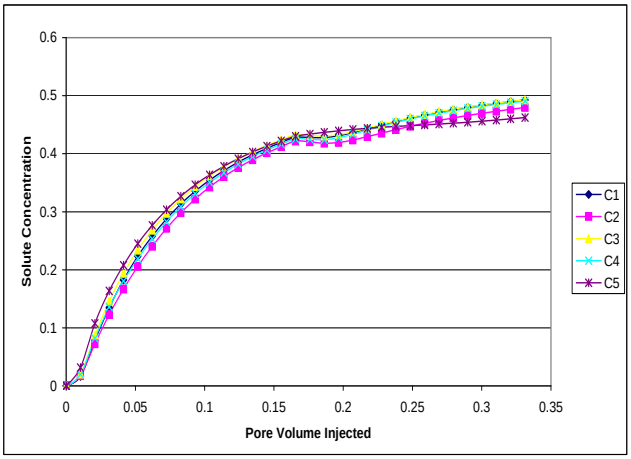

(a) Breakthrough curves at points C1—C5, 0.6 meters ACL: Simulation E1

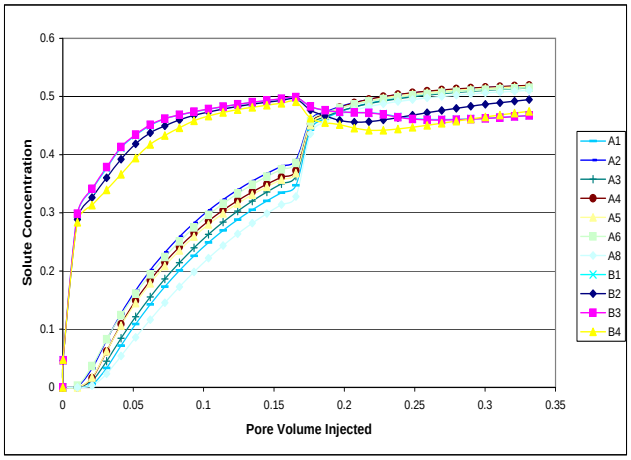

(b) Breakthrough curves at well locations, 0.6 meters ACL: Simulation E1

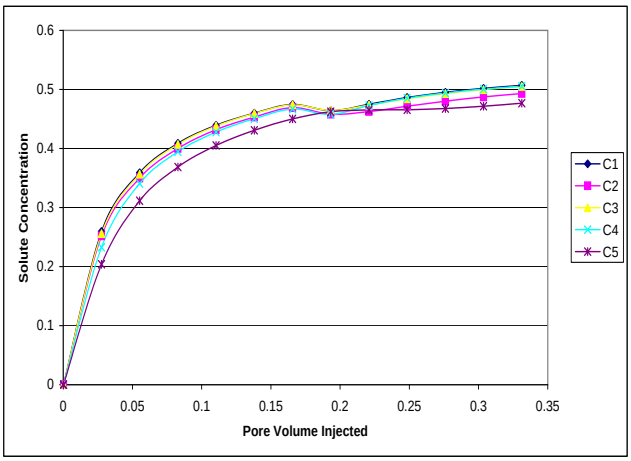

(c) Breakthrough curves at points C1—C5, at the clay layer surface: Simulation E11

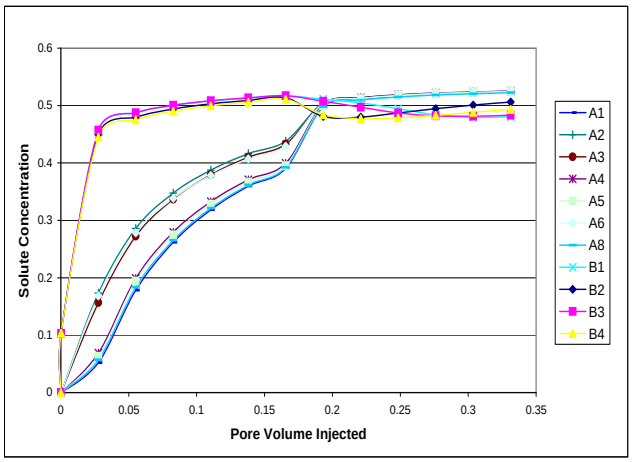

(d) Breakthrough curves at well locations, at the clay layer surface: Simulation E11

Figure 5.4: Breakthrough curves: Simulations E1 and E11

In an ideal brine emplacement, all solute injected would remain in the lower portion of the domain, or within the layer that a brine barrier is desired. In addition, the brine layer would be stratified, or have no variance in concentration at a constant height. However, subsurface heterogeneity and instabilities that form during the injection process diminish efficiency. The analyses conducted utilize these assumptions for an ideal establishment of a brine barrier to investigate the efficiency of brine emplacement under various circumstances. Therefore, to evaluate the formation of a brine layer, the variance in concentration and the average concentration across horizontal planes were monitored over time.

The variances in concentration seen at four elevations, in each simulation, are shown in Figures 5.5(a)—5.5(d). Thereafter, Table 5.1 provides the variance in concentration at given heights within the lower 0.6 meters of the domain, averaged over time. The simulations are listed in order of increasing variance to represent the rank of efficiency. Recall that simulations E1—E6 represent a low-rate (LR) brine injection of 0.010 PV day^{-1}, while simulations E6—E12 represent a high-rate (HR) brine injection of 0.028 PV day^{-1}.

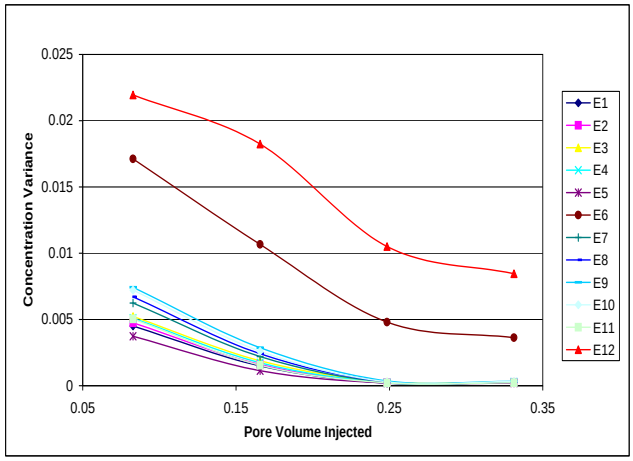

(a) Variance in concentration across the domain at clay layer surface

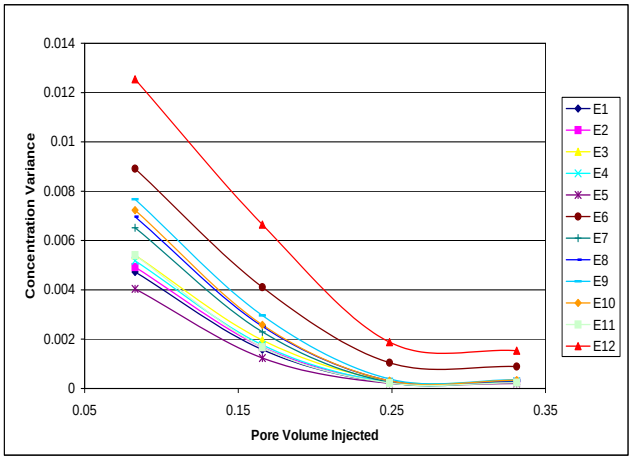

(b) Variance in concentration across the domain at a height 0.15 meters ACL

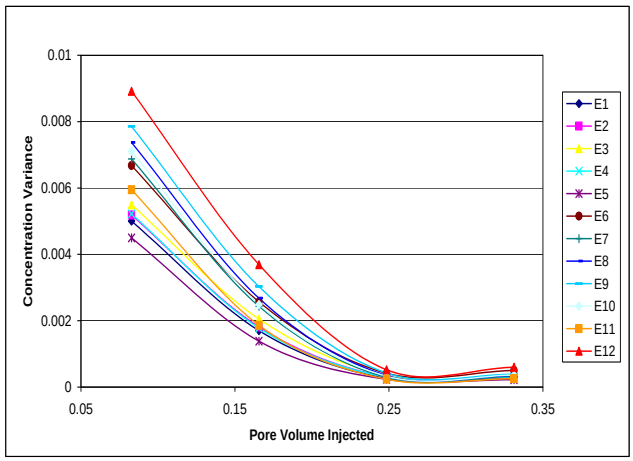

(c) Variance in concentration across the domain at a height 0.30 meters ACL

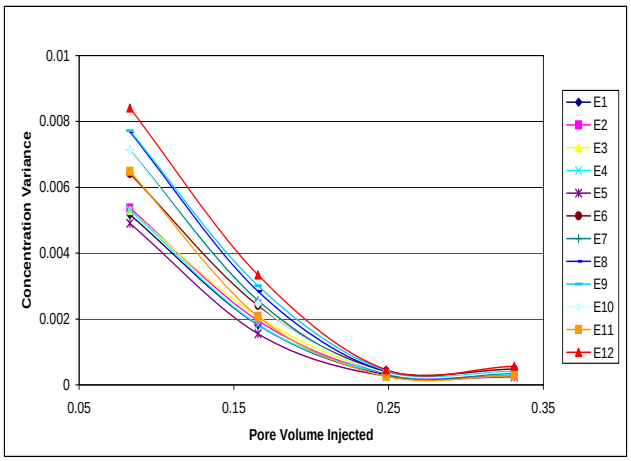

(d) Variance in concentration across the domain at a height 0.45 meters ACL

Figure 5.5: Variance in concentration at various heights in simulations E1—E12

The following observations can be made from analysis of Figures 5.5(a)—5.5(d):

1. Initially, different concentration variance values are seen among the simulations, though the degree of heterogeneity is not indicative of the amount of concentration variation. For example, the concentration variance seen in the homogeneous simulation E1 is consistently less than that seen in simulation E3 (Gaussian SRF, $\sigma_Y^2 = 1$) but consistently greater than that seen in simulation E5 (layered, $\sigma_Y^2 = 1$).

2. Excluding the two simulations in which $\sigma_Y^2 = 2$ (E6 and E12), the concentration variance values, which initially range between 0.00373 and 0.00743, converge after 0.25 pore volume is injected.

Table 5.1: Variance in concentration (σ_c^2) at given heights ACL averaged over the injection period

0.00 m ACL		0.15 m ACL		0.30 m ACL		0.45 m ACL		0.60 m ACL	
Sim	σ_c^2	Sim	σ_c^2	Sim	σ_c^2	Sim	σ_c^2	Sim	σ_c^2
E5	0.0013	E5	0.0014	E5	0.0016	E5	0.0017	E5	0.0016
E1	0.0016	E1	0.0017	E1	0.0018	E1	0.0019	E1	0.0019
E2	0.0017	E2	0.0018	E2	0.0019	E4	0.0020	E4	0.0019
E11	0.0018	E4	0.0019	E4	0.0019	E2	0.0020	E3	0.0019
E4	0.0018	E11	0.0019	E3	0.0021	E3	0.0020	E2	0.0020
E3	0.0019	E3	0.0020	E11	0.0021	E11	0.0023	E11	0.0022
E7	0.0022	E7	0.0023	E7	0.0025	E6	0.0024	E6	0.0024
E8	0.0024	E8	0.0025	E6	0.0025	E10	0.0026	E10	0.0026
E10	0.0026	E10	0.0026	E10	0.0026	E7	0.0026	E7	0.0026
E9	0.0027	E9	0.0028	E8	0.0027	E8	0.0028	E9	0.0028
E6	0.0091	E6	0.0037	E9	0.0029	E9	0.0029	E8	0.0028
E12	0.0148	E12	0.0057	E12	0.0034	E12	0.0032	E12	0.0030

3. In the upper half of the injection area, the concentration variance values of all simulations converge after 0.25 pore volume is injected.

The variance patterns in Figures 5.5(a)—5.5(d) imply that, if a sufficient brine layer can be reached before 0.25 pore volume is injected, an injection rate of 0.010 PV day^{-1} is more optimal than 0.028 PV day^{-1}. This will result in less brine mounding which is necessary to proceed to the subsequent stage of BBRT. However, if a layer of sufficient concentration is not expected to be reached before the change in variance tends to zero (or before 0.25 PV is injected), then injection rate will not be the most important factor in brine layer formation. As the volume required to reach a barrier of specified concentration increases, the mounds which have formed have more time to dissipate. In this case, a HR may be beneficial to expedite the emplacement process.

Table 5.1 suggests that injection rate is dominant over subsurface heterogeneity as a factor in the determination of concentration variance when the heterogeneity of the ln permeability is less than 1. With the exception of E11 and E6, the variance is smaller in each of the LR simulations than in any HR simulations. Although E11 and E6 are outliers, the variance in E11

is consistently smaller than in E5 (the LR simulation with a corresponding permeability field), and the same relationship is seen between E6 and E12.

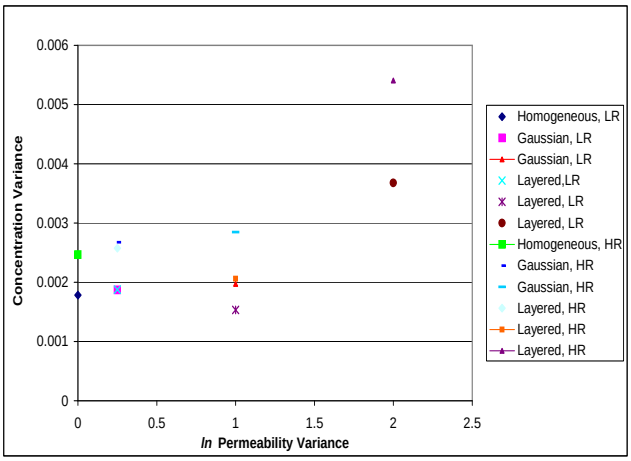

(a) Horizontal concentration variance averaged over time and space as a function of *ln* permeability variance

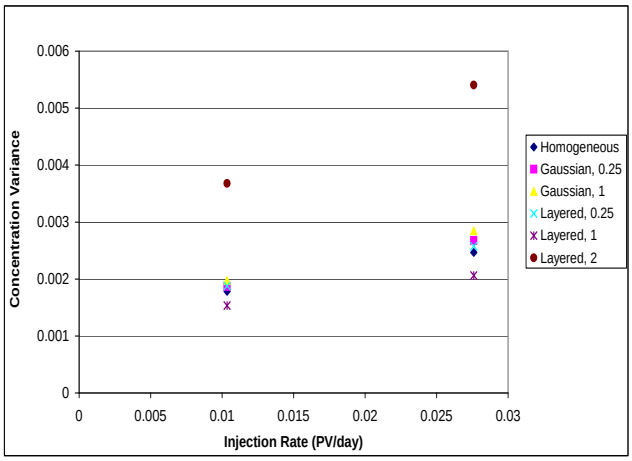

(b) Horizontal concentration variance averaged over time and space as a function of injection rate

Figure 5.6: Average variance in concentration throughout injection period as a function of (a) *ln* permeability and (b) injection rate

Figures 5.6(a) and 5.6(b) show the horizontal variance in concentration, averaged over time and over elevations up to 0.6 meters ACL, as a function of both heterogeneity and injection rate. Though not shown, various plots were generated for specific elevations and injection times. Because similar patterns were seen among these plots, the average is used as a representation. The figures suggest that, for moderately heterogeneous domains, concentration variance is more greatly dependent on injection rate than on the degree of subsurface heterogeneity. With the exception of the two highly heterogeneous simulations, E6 and E12, a greater amount of variation is seen among simulations with the same permeability field than among simulations with the same injection rate. Therefore, in moderately heterogeneous cases, the rate of brine emplacement has a greater effect on brine mounding than does the heterogeneity of subsurface permeability.

The concentration of the brine layer necessary for BBRT depends on the density of the DNAPL being removed. Therefore, concentration profiles are equally as important as concentration variances in determining the efficiency of brine emplacement scenarios. Figures 5.7(a)—5.7(d) represent average concentrations through four horizontal slices of the domain from simu-

lations E1—E12. Since the density of DNAPL used in the pilot study of BBRT was 1.6 g mL^{-1}, the brine barrier concentration necessary was 0.48 kg kg^{-1}.

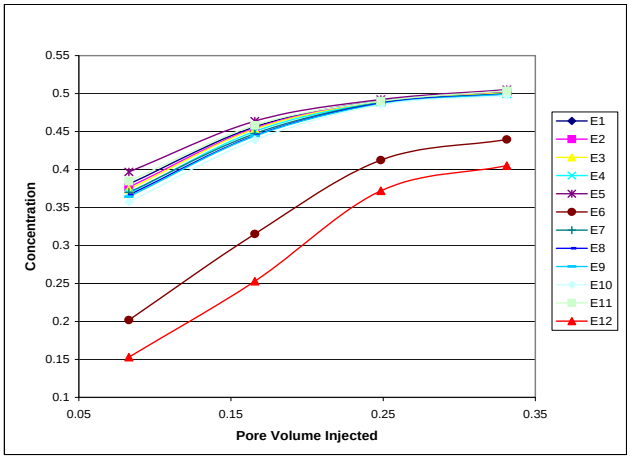

(a) Average concentration across the domain at the clay layer surface

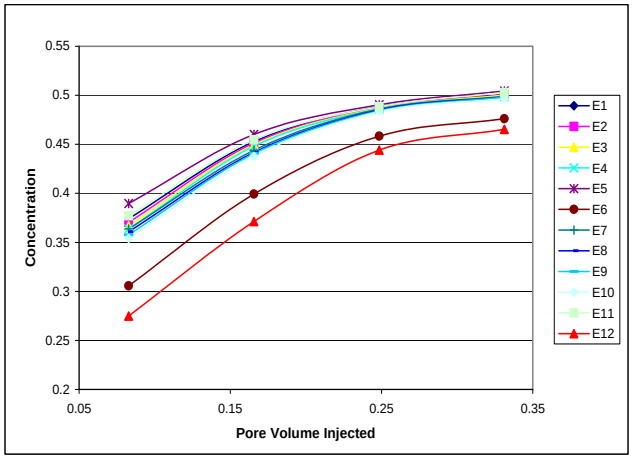

(b) Average concentration across the domain at a height 0.30 meters ACL

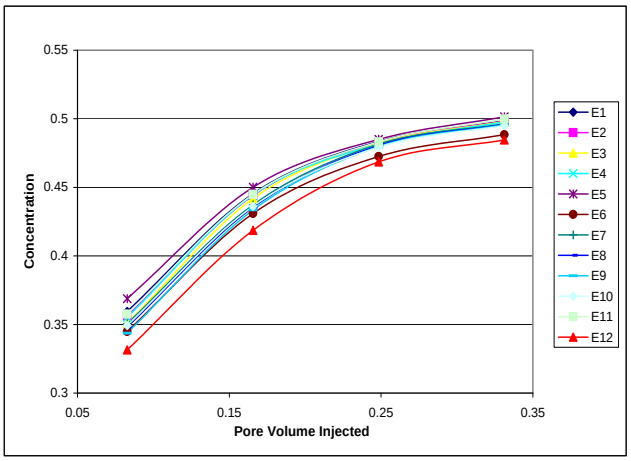

(c) Average concentration across the domain at a height 0.45 meters ACL

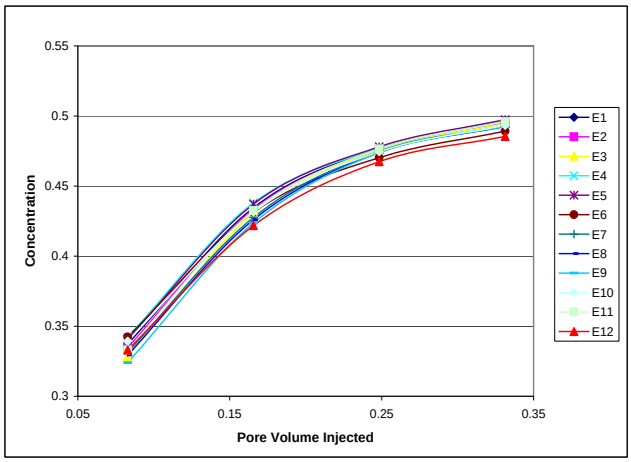

(d) Average concentration across the domain at a height 0.60 meters ACL

Figure 5.7: Average concentration across the domain at various heights

An "effective concentration" was calculated by subtracting the standard deviation across a plane from the average concentration. It was assumed that this value could conservatively represent the concentration of brine at a given elevation. Using this analysis, it was concluded that simulations E1—E4 all reached a concentration of 0.48 kg kg^{-1} up to 0.3 meters ACL after 0.33 pore volume was injected. Simulations E5 and E11 resulted in sufficient brine barriers up to a height of 0.45 meters ACL after the same volume was injected. After termination, a sufficient brine barrier was yet to be established in the remaining simulations. This can be explained by

analysis of Table 5.2.

Table 5.2 provides the average concentration over time at various elevations to show the general trends in concentration comparisons between simulations. The simulations are listed in order of decreasing concentration. The table can be used to analyze the amount of brine in the lower half of the injection area relative to that in the upper half. The numbers demonstrate that the ratio of mass between 0.0 and 0.3 meters ACL to mass between 0.3 and 0.6 meters ACL is greater in the LR simulations than in the HR simulations, with the exception again of simulations E11 and E6. It is observed that the higher injection rate causes more solute mass to travel upward through the domain than does the lower injection rate. This suggests that the LR simulations are more efficient than the HR simulations, as the brine layer is intended to form on the clay layer at the bottom of the injection area.

Table 5.2: Concentration at given heights ACL averaged over the injection period

0.00 m ACL		0.15 m ACL		0.30 m ACL		0.45 m ACL		0.60 m ACL	
Sim	Conc	Sim	Conc	Sim	Conc	Sim	Conc	Sim	Conc
E5	0.465	E5	0.461	E5	0.451	E5	0.438	E6	0.427
E11	0.459	E11	0.456	E1	0.447	E4	0.438	E4	0.425
E1	0.457	E11	0.454	E11	0.446	E1	0.436	E10	0.424
E2	0.456	E2	0.452	E2	0.445	E2	0.435	E12	0.422
E3	0.454	E3	0.451	E4	0.445	E10	0.435	E1	0.421
E4	0.452	E4	0.449	E3	0.443	E11	0.435	E2	0.421
E7	0.451	E7	0.448	E7	0.441	E6	0.433	E5	0.420
E8	0.450	E8	0.447	E8	0.440	E3	0.432	E7	0.419
E9	0.449	E9	0.445	E10	0.440	E7	0.432	E3	0.419
E10	0.445	E10	0.443	E9	0.438	E8	0.431	E8	0.418
E6	0.342	E6	0.410	E6	0.434	E9	0.429	E11	0.417
E12	0.296	E12	0.389	E12	0.426	E12	0.427	E9	0.417

Combining analysis of concentration variance and average concentration, it was concluded that the most heterogeneous domains (those with a ln permeability variance equal to 2) were the least efficient overall. In BBRT implementation, systems of this type may require considerably more time and brine injection. However, strong conclusions can not be made from the simulations, since only one representation of a heterogeneity field with $\sigma_Y^2 = 2$ was used. Analysis of the

randomly generated field did indeed show that a value of relatively low permeability was used for the bottom layer of the domain. This is assumed to have contributed, in simulations E6 and E12, to the high variances in concentration seen at lower elevations and to the relatively large amount of solute which moved upward into the domain.

In the moderately heterogeneous and homogeneous simulations, the efficiency was more dependent on injection rate than on the degree of heterogeneity. HR simulations reached similar concentrations as the corresponding LR simulations after an average additional of 0.08 pore volume was injected. Though HR simulations reach a given volume sooner than LR simulations, the brine mounding that ensues may take an undesirable amount of time to relax and dissipate.

5.3 Brine Recovery Simulations

Simulations representing brine recovery were performed to evaluate the effects of heterogeneity and extraction rate on solute recovery. A total of 0.33 PV of fluid was extracted over a period of 32 days in the low rate (LR) simulations, 18 days in the medium rate (MR) simulations and 12 days in the high rate (HR) simulations. Two methods of simultaneous flushing were considered among the simulations—one in which freshwater was injected at points along the top of the saturated zone, hereafter referred to as the upper flush (UF), and another in which freshwater was injected at points directly above the clay layer but away from extraction wells, or a lower flush (LF).

Solute concentrations at well effluents were monitored over time. Conversion of these concentrations to corresponding mass removal rates allowed for numerical integration to approximate the solute mass removed. The general trends found in these values can be seen in Figure 5.8. Fractional solute recovered from a domain containing approximately 5,598 kg solute (or 0.17 PV of fully concentrated brine) was used to compare the efficiency of brine recovery between simulations.

Initial analysis concluded that each UF simulation was more efficient than every LF sim-

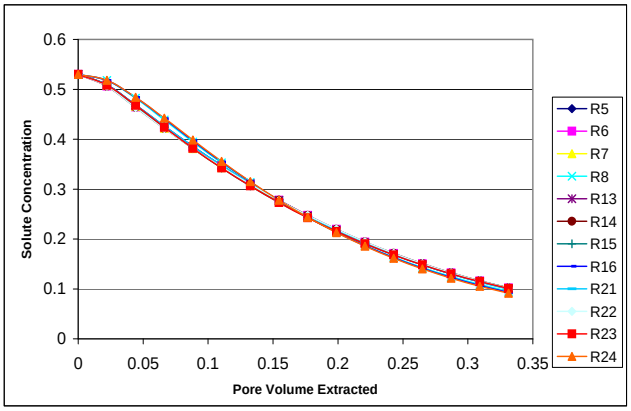

(a) Average concentration at effluents in UF simulations

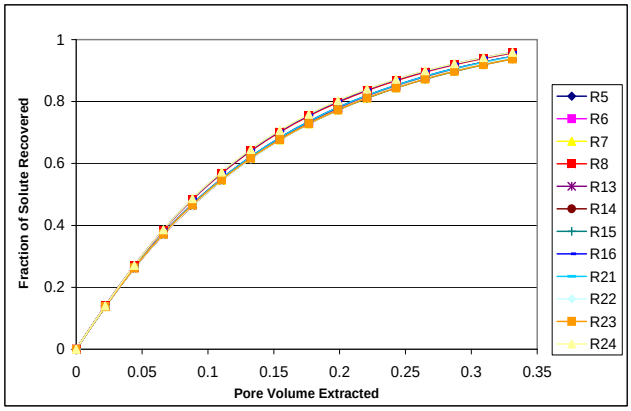

(b) Fractional solute mass removed in UF simulations

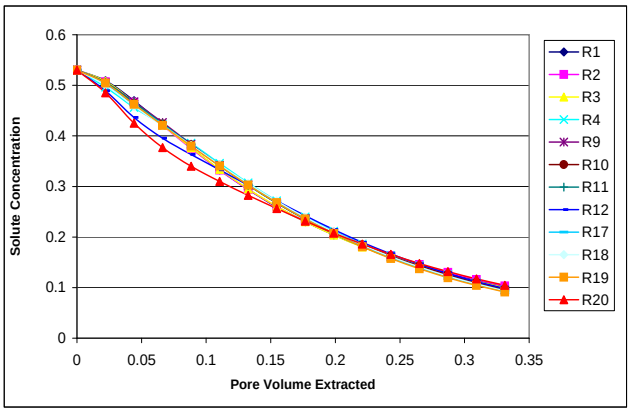

(c) Average concentration at effluents in LF simulations

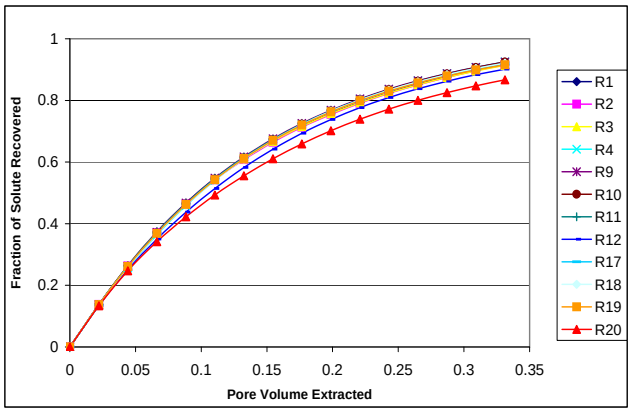

(d) Fractional solute mass removed in LF simulations

Figure 5.8: Average concentration at effluents and fractional solute mass removed in recovery simulations

ulation. The average fraction of solute mass removed in the UF simulations was 0.946, with a variance of 6.04×10^{-5}, and the average removed in the LF simulations was 0.914, with a variance of 2.60×10^{-4}. Individual simulation results are represented in Table 5.3 (UF) and Table 5.5 (LF), in which they are listed in decreasing order of solute fraction removed during brine recovery. Because it was apparent that the most dominant factor in efficiency among the simulations was the flushing method, analyses of the impacts of subsurface heterogeneity and extraction rate variation were conducted on the LF and UF scenarios independently.

Analysis of Table 5.3 suggests that, using the UF scenario, an increase in heterogeneity does not correspond to an increase or decrease in brine extraction efficiency. All simulations conducted with Gaussian and layered permeability fields with $\sigma_Y^2 = 0.25$ resulted in less solute

Table 5.3: Fractional mass removed in upper flush simulations

Simulation	% Solute Removed	Domain	Variance	Rate
R24	95.89	Layered	1	High
R16	95.84	Layered	1	Medium
R8	95.66	Layered	1	Low
R21	94.59	Homogeneous	0	High
R13	94.56	Homogeneous	0	Medium
R5	94.56	Homogeneous	0	Low
R6	94.33	Gaussian	0.25	Low
R14	94.24	Gaussian	0.25	Medium
R22	94.18	Gaussian	0.25	High
R7	93.91	Layered	0.25	Low
R15	93.76	Layered	0.25	Medium
R23	93.74	Layered	0.25	High

removal than did the homogeneous simulations. However, the simulations conducted in which the heterogeneity was layered and σ_Y^2 =1 resulted in the greatest amount of solute removal. This suggests that a knowledge of simply the variance of heterogeneity will not allow for the prediction the brine removal efficiency.

The grouping of heterogeneity fields in Table 5.3 implies that the specific subsurface field is the dominant factor in the amount of solute removed. Though the degree of overall heterogeneity may not be the determining factor in brine removal efficiency, the specific location and orientation of low permeability and high permeability areas may have a large impact on recovery. Therefore, since the difference in an extraction rate of 0.010 PV day^{-1} and 0.028 PV day^{-1} is negligible compared to the effects of subsurface variation, a high extraction rate can efficiently be utilized to expedite the recovery process.

Figures 5.9(a) and 5.9(b) demonstrate the fractional solute mass removed in UF simulations as a function of (a) *ln* permeability variance and (b) extraction rate. Table 5.4 provides the variance between the groups of simulations represented in Figures 5.9(a) and 5.9(b). Analysis of these figures further suggests that brine recovery efficiency is more dependent on subsurface

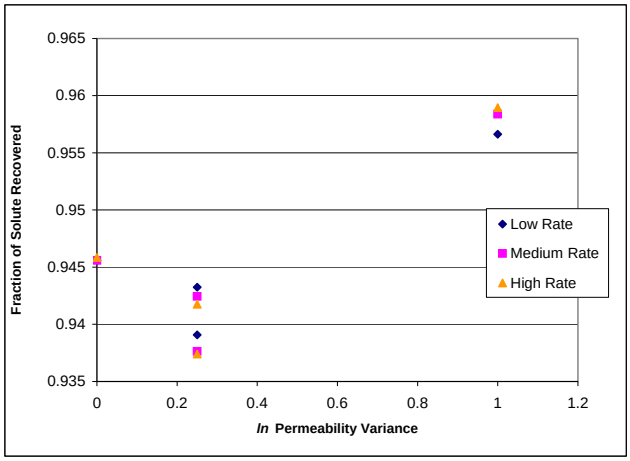

(a) Solute recovery as a function of *ln* permeability in UF simulations

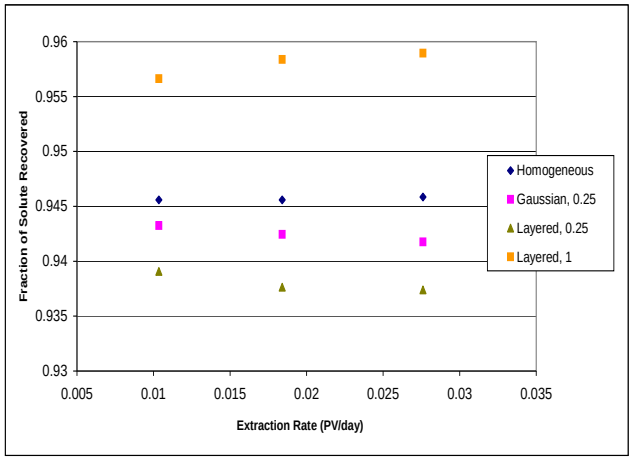

(b) Solute recovery as a function of extraction rate in UF simulations

Figure 5.9: Solute recovery in UF simulations

Table 5.4: Variance in solute recovery among groups of UF simulations

UF Simulation Group	σ^2 in Solute Recovery
Low Rate	5.62×10^{-5}
Medium Rate	7.86×10^{-5}
High Rate	8.66×10^{-5}
Homogeneous	2.17×10^{-8}
Gaussian, σ^2=0.25	5.60×10^{-7}
Layered, σ^2=0.25	8.32×10^{-7}
Layered, σ^2=1.0	1.45×10^{-7}

heterogeneity than on the rate of brine removal. The variances in solute recovery among simulations with equivalent permeability fields are at least two orders of magnitude less than those among simulations with a constant extraction rate. This finding is contrary to the results seen in the brine emplacement simulations.

Equivalent analysis was conducted on LF simulations, though correlations were less apparent. Table 5.5 provides LF simulations listed in order of decreasing fractional solute mass removed. Unlike the pattern seen in the UF simulations, each specific permeability field does not correspond to a rank of brine removal efficiency.

Table 5.5: Fractional mass removed in lower flush simulations

Simulation	% Solute Removed	Domain	Variance	Rate
R4	92.50	Layered	1	Low
R9	92.48	Homogeneous	0	Medium
R10	92.46	Gaussian	0.25	Medium
R18	92.11	Gaussian	0.25	High
R11	92.01	Layered	0.25	Medium
R17	91.95	Homogeneous	0	High
R1	91.66	Homogeneous	0	Low
R19	91.56	Layered	0.25	High
R2	91.53	Gaussian	0.25	Low
R3	91.36	Layered	0.25	Low
R12	90.15	Layered	1	Medium
R20	86.68	Layered	1	High

Figures 5.10(a) and 5.10(b) were generated to assess the solute recovery as a function of *ln* permeability variance and extraction rate. Values for the variance in solute recovery between the simulation groups represented in these figures are presented in Table 5.6. Again, no strong correlation is seen, and the results are inconclusive. However, a more comprehensive investigation is unnecessary as it has been concluded that UF schemes are more optimal than LF schemes.

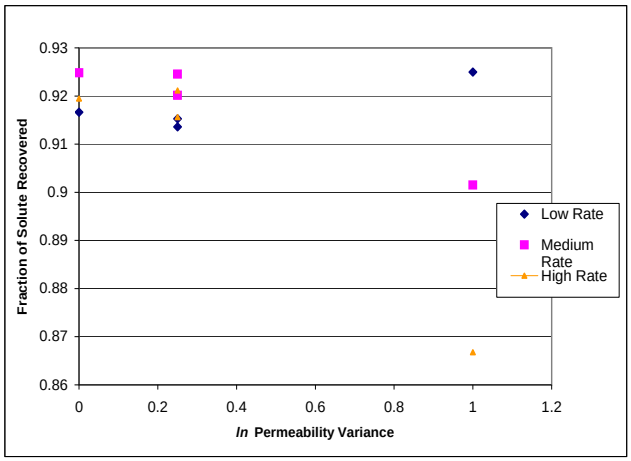

(a) Solute recovery as a function of *ln* permeability in LF simulations

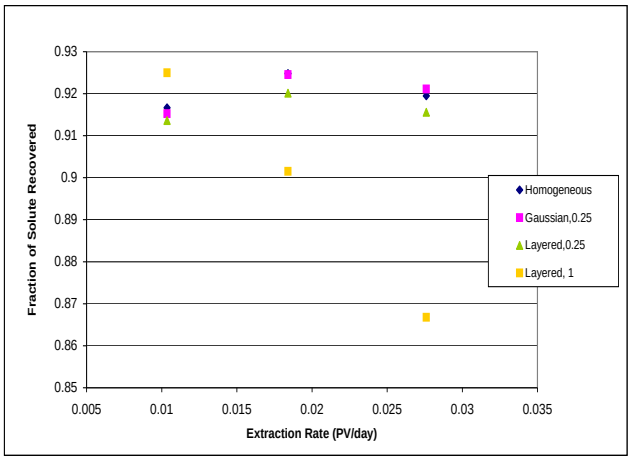

(b) Solute recovery as a function of extraction rate in LF simulations

Figure 5.10: Solute recovery in LF simulations

Figures 5.11(a) and 5.11(b) are concentration profiles, generated using SutraPlot, shown to represent instabilities seen in homogeneous LR simulations using (a) a UF scheme and (b)

Table 5.6: Variance in solute recovery among groups of LF simulations

LF Simulation Group	σ^2 in Solute Recovery
Low Rate	2.55×10^{-5}
Medium Rate	1.22×10^{-4}
High Rate	6.80×10^{-4}
Homogeneous	1.71×10^{-5}
Gaussian, σ^2=0.25	2.21×10^{-5}
Layered, σ^2=0.25	1.12×10^{-5}
Layered, σ^2=1.0	8.57×10^{-4}

a LF scheme. These figures are provided to demonstrate a possible reason for the decreased efficiency among LF simulations. Though both scenarios produce instabilities, it appears that the LF scheme allows a much greater amount of solute mass to remain in the upper portion of the domain.

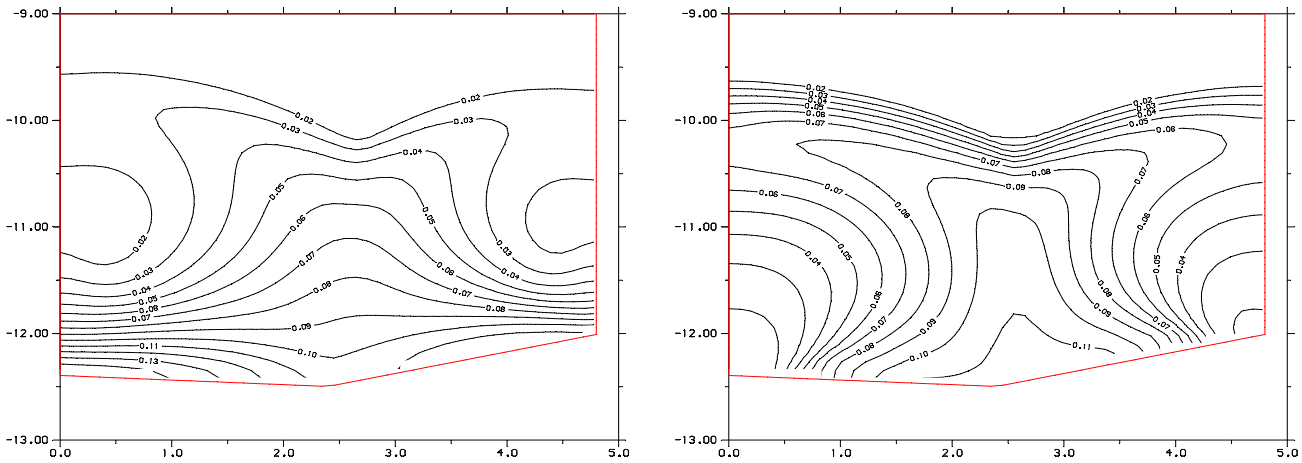

(a) Concentration profile: UF simulation R5

(b) Concentration profile: LF simulation R1

Figure 5.11: Instabilities in concentration in homogeneous recovery simulations

5.4 Viscosity Simulations

5.4.1 Set 1 Simulations

The first set of viscosity simulations was performed to analyze the independent effects of viscosity and density as brine displaces freshwater horizontally, as is seen in the brine emplacement stage of BBRT. As mathematical modeling of brine processes are important for BBRT implementation, it is beneficial to evaluate the impacts of assumptions made by common groundwater flow and transport models, such as linearly varying density or negligible viscosity changes.

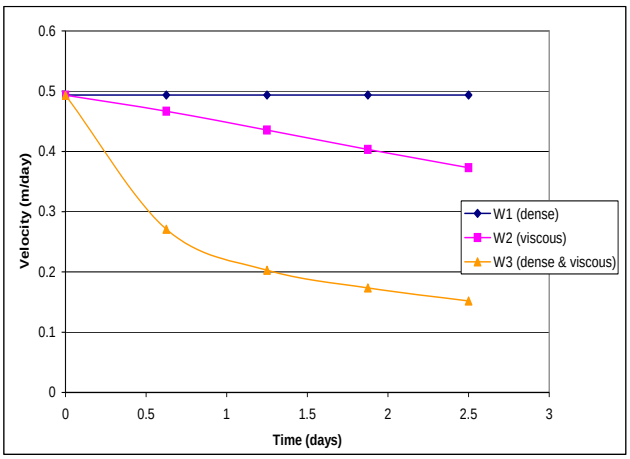

(a) Average horizontal velocity in Set 1 homogeneous simulations

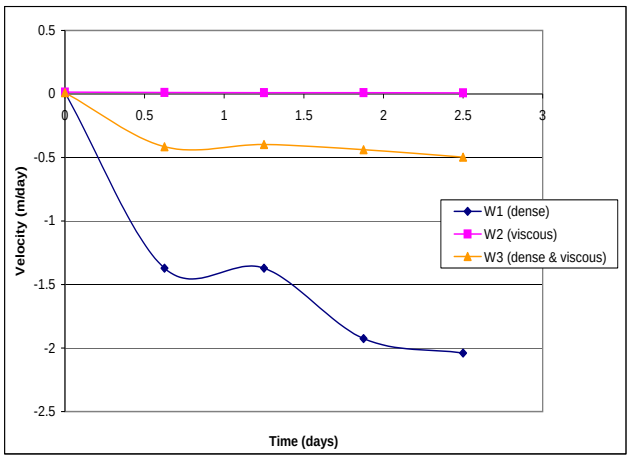

(b) Average vertical velocity in Set 1 homogeneous simulations

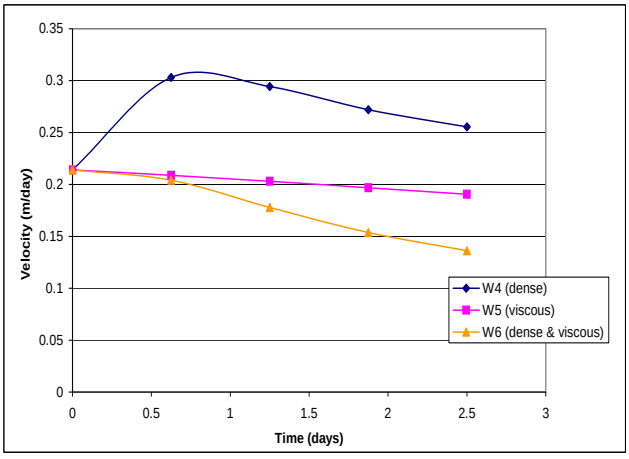

(c) Average horizontal velocity in Set 1 heterogeneous simulations

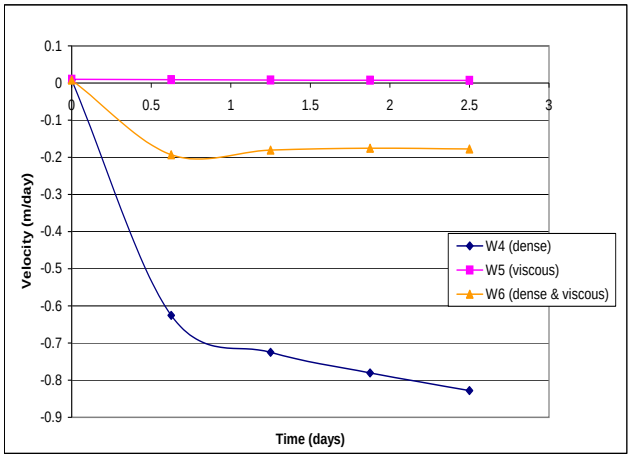

(d) Average vertical velocity in Set 1 heterogeneous simulations

Figure 5.12: Average horizontal and vertical velocities in Set 1 simulations

Figures 5.12(a)—5.12(d) show the average horizontal and vertical velocities in the Set 1 simulations. Vertical velocities are represented as negative values to indicate a downward flow.

The following observations can be made from the figures:

1. In homogeneous simulations, the horizontal velocity was seen to depend only on the viscosity of the fluid (Figure 5.12(a)). As time increased and solute moved into the domain, the fluid in which viscosity was held constant (W1) encountered no change in horizontal velocity. However, when the viscosity equation of state was added to the model, the horizontal velocity after 2.5 days was seen to decrease by 24% when density changes were neglected (W2) and to decrease by 70% when density changes were accounted for (W3).

2. In homogeneous simulations, the vertical velocity was seen to depend only on the density of the fluid (Figure 5.12(b)). As solute moved into the domain, no change in vertical velocity was observed for the fluid in which density was held constant (W2). After 2.5 days, a dense yet non-viscous fluid (W1) encountered an increase in vertical velocity of 2.04 m day^{-1}, while a dense and viscous fluid (W3) encountered an increase of 0.50 m day^{-1}.

3. The effect of viscosity on horizontal velocity was increased when density effects were added. The horizontal velocity of the dense and viscous fluid decreased more rapidly than did the viscous fluid.

4. When combined with viscous effects, the rate at which density caused the fluid's vertical velocity to increase was minimized.

5. As can be seen in Figures 5.12(c) and 5.12(d), the added complexities of subsurface heterogeneity had a significant impact on velocity. Horizontal velocity was no longer dependent solely on viscosity and was, on average, approximately half the rate of that seen in homogeneous simulations. Vertical velocity was still largely dependent on density, yet velocity was sill approximately half that seen in homogeneous simulations.

These observations demonstrate the importance of accounting for density and viscosity variations when modeling a fluid with behavior similar to $CaBr_2$. As can be seen from velocity

profiles, the negligence of viscosity changes leads to an overestimation of both horizontal and vertical flow, while the negligence of density variations results in an overestimation of horizontal flow and the underestimation of vertical flow.

Homogeneous concentration profiles are not shown because uniform flow, which can be conceptualized by Figures 5.12(a) and 5.12(b), was observed. However, the use of a heterogeneous domain, seen in Figure 5.13, resulted in interesting solute transport patterns. Figures 5.14(a)—5.14(c) provide profiles seen after 0.625 days across the vertical plane $z = 0.1$ meters. Comparison of Figure 5.13 to the Figures 5.14(a) and 5.14(c) demonstrates the shorter solute travel distance seen near the origin, in which a low permeability region exists. However, the concentration profile for the viscous, non-dense brine does not appear to be as greatly impacted by the low permeability region.

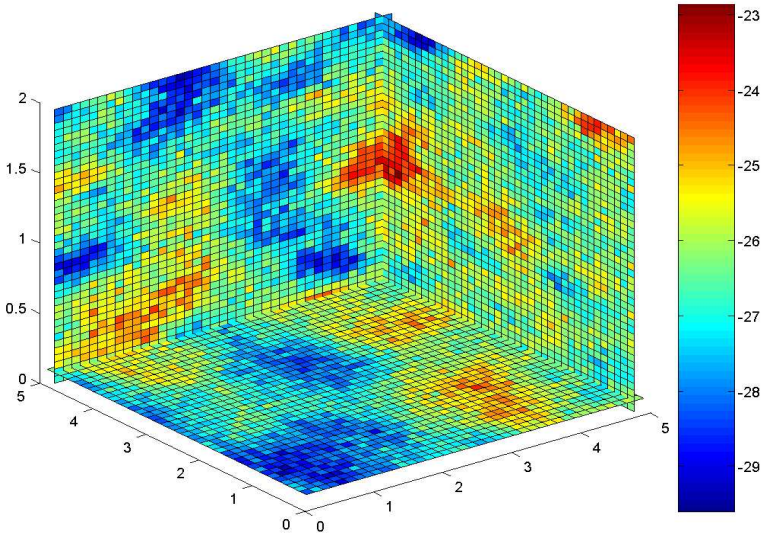

Figure 5.13: *ln* permeability field, profile of [4.8,4.8.0.1] meters : Set 1 heterogeneous simulations

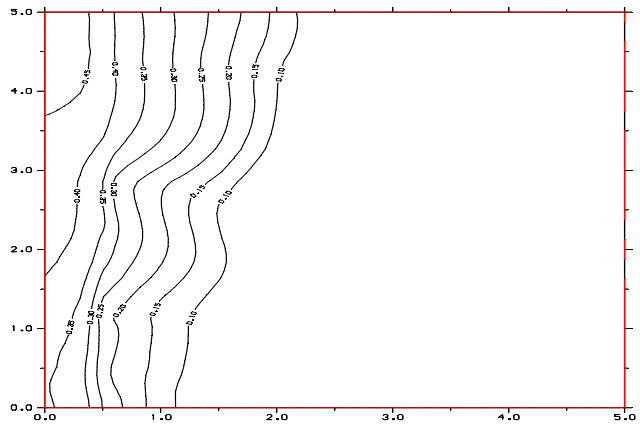

(a) Concentration profile at $z = 0.1$ m after 0.625 days: simulation W4

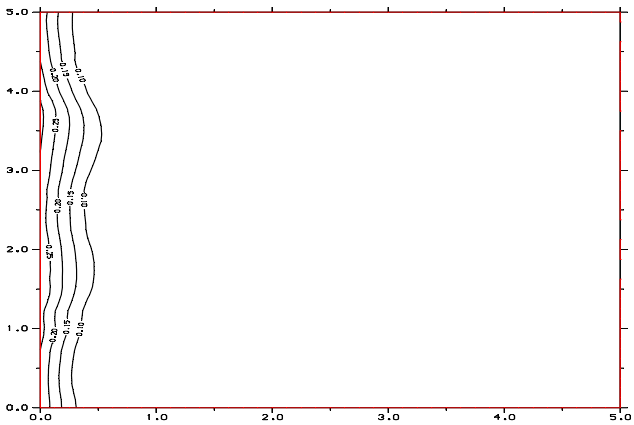

(b) Concentration profile at $z = 0.1$ m after 0.625 days: simulation W5

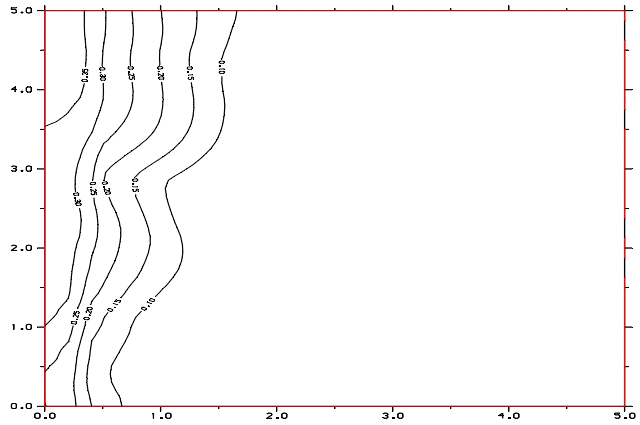

(c) Concentration profile at $z = 0.1$ m after 0.625 days: simulation W6

Figure 5.14: Concentration profiles from heterogeneous Set 1 simulations

5.4.2 Set 2 Simulations

The second set of viscosity simulations examined the effects of density and viscosity on the displacement of brine by freshwater. The simulations are representative of the upper flush of freshwater performed in the brine recovery process. Similar analysis was conducted, in which the average velocity over time was monitored and compared between systems in which solute concentration had different effects. Figures 5.15(a)—5.15(d) demonstrate the average horizontal and vertical velocities seen in the Set 2 simulations. Both horizontal and vertical velocities remained relatively constant over time in all simulations. This suggests that the enforced pressure boundaries may have had a larger impact on fluid flow than did the displacing freshwater. For this reason, an analysis of the magnitude of viscosity and density effects over time could not be conducted. However, a comparison of the velocities of the three types of fluids was useful. Analysis of Figures 5.15(a)—5.15(d) suggest the following:

1. In homogeneous simulations, horizontal velocity of a dense fluid was 38.7 times greater than a viscous, non-dense fluid and was 5.1 times greater than a dense and viscous fluid.

2. In homogeneous simulations, vertical velocity of a dense fluid was 127.3 times greater than a viscous, non-dense fluid and was 5.1 times greater than a dense and viscous fluid.

3. In heterogeneous simulations, horizontal velocity of a dense fluid was 22.8 times greater than a viscous, non-dense fluid and was 5.6 times greater than a dense and viscous fluid.

4. In heterogeneous simulations, vertical velocity of a dense fluid was 52.9 times greater than a viscous, non-dense fluid and was 4.6 times greater than a dense and viscous fluid

5. Horizontal velocity in a given homogeneous simulations was, on average, 7.4 times greater than in the corresponding heterogeneous simulation. Vertical velocity in a given homogeneous simulations was, on average, 1.8 times greater. However, since only one random

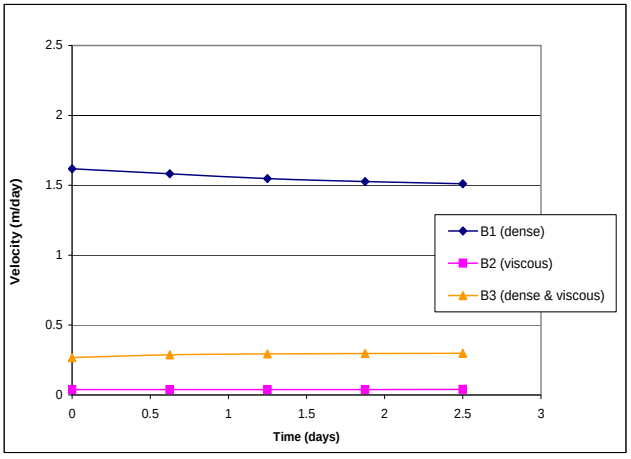

(a) Average horizontal velocity in Set 2 homogeneous simulations

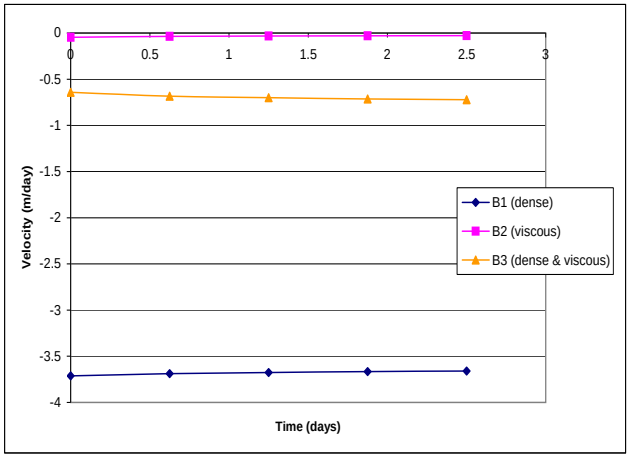

(b) Average vertical velocity in Set 2 homogeneous simulations

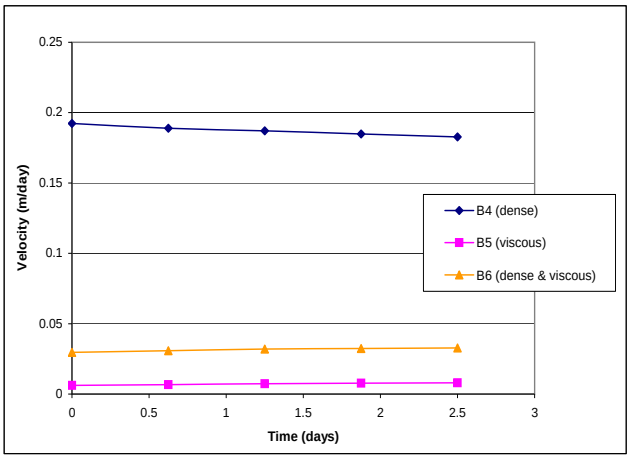

(c) Average horizontal velocity in Set 2 heterogeneous simulations

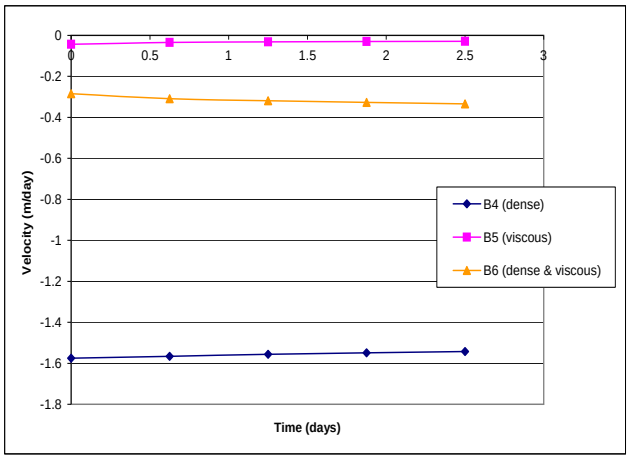

(d) Average vertical velocity in Set 2 heterogeneous simulations

Figure 5.15: Average horizontal and vertical velocities in Set 2 simulations

permeability field was utilized, this result can not be assumed to be indicative of heterogeneous domains with a similar degree of heterogeneity.

The velocity profiles demonstrate the impacts of density and viscosity on fluid velocities, and stress the importance of including both effects in flow and transport modeling. As suggested by Figures 5.15(a)—5.15(d), neglecting a change in viscosity with concentration variation will lead to the overestimation of horizontal and vertical flow. In addition, negligence of density changes will lead to an underestimation of horizontal and vertical fluid velocities.

Figures 5.16(a)—5.16(c) show concentration profiles from the homogeneous simulations, which represent solute travel resulting from velocity patterns given previously. The profiles also

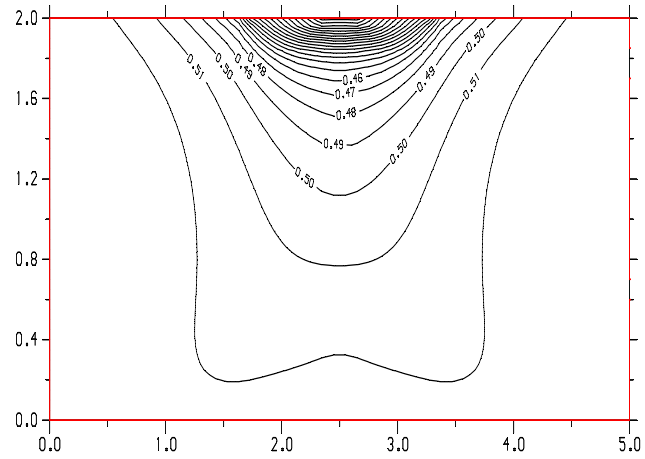

(a) Concentration profile at $y = 2.5$ m after 1.25 days: simulation B1

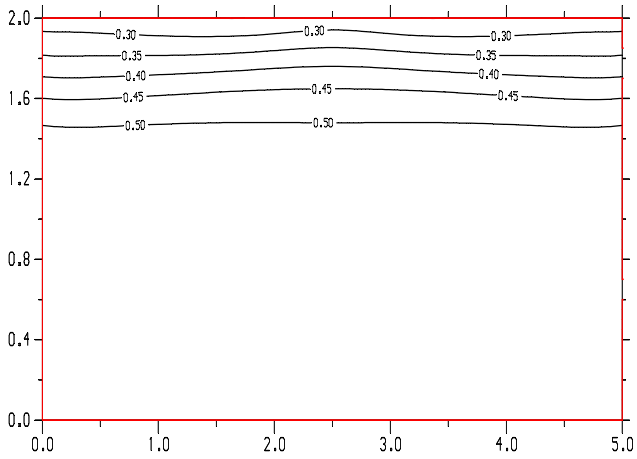

(b) Concentration profile at $y = 2.5$ m after 1.25 days: simulation B2

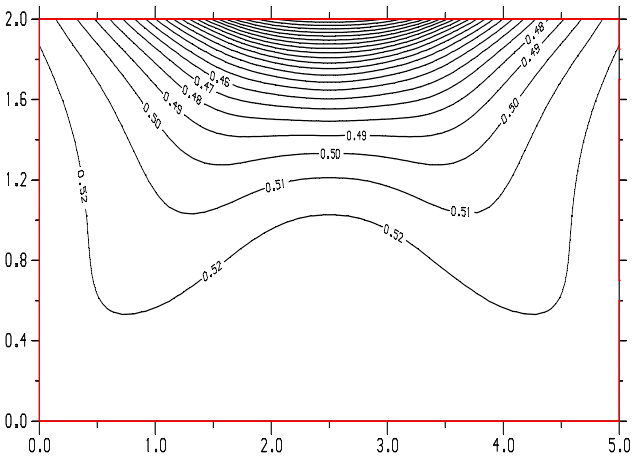

(c) Concentration profile at $y = 2.5$ m after 1.25 days: simulation B3

Figure 5.16: Concentration profiles from homogeneous Set 2 simulations

demonstrate instabilities which form as dense fluid is displaced by less dense fluid (Figures 5.16(a) and 5.16(c)). The instabilities are not seen in 5.16(b), the system in which density differences were neglected.

Figures 5.18(a)—5.18(c) give concentration profiles from heterogeneous simulations utilizing the Gaussian random field shown in Figure 5.17. Visual comparison of the figures shows the instabilities propagating near high permeability areas and diffusing in the vicinity of low permeability regions. As was seen in the Set 1 simulations, it appears that the system in which brine was represented as viscous and non-dense (B5) was less affected by the heterogeneity than were the other systems.

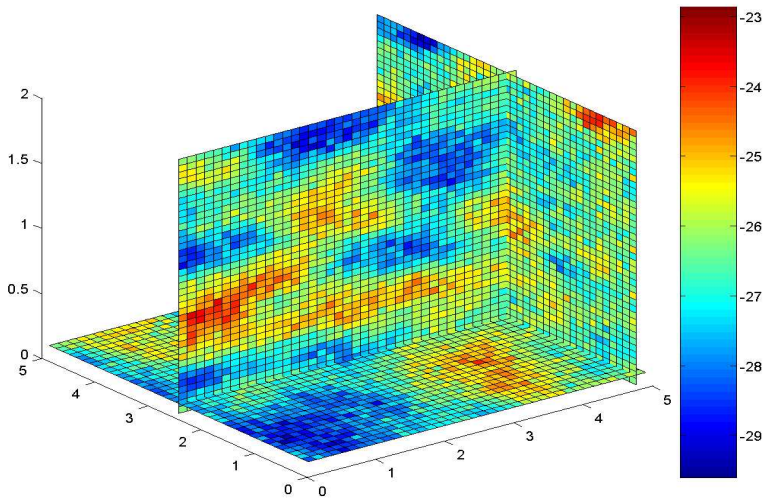

Figure 5.17: *ln* permeability field, profile of [4.8,2.5,0.1] meters: Set 2 heterogeneous simulations

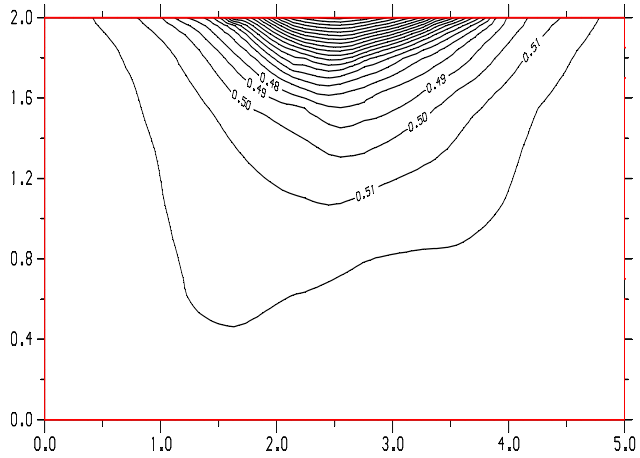

(a) Concentration profile at $y = 2.5$ m after 1.25 days: simulation B4

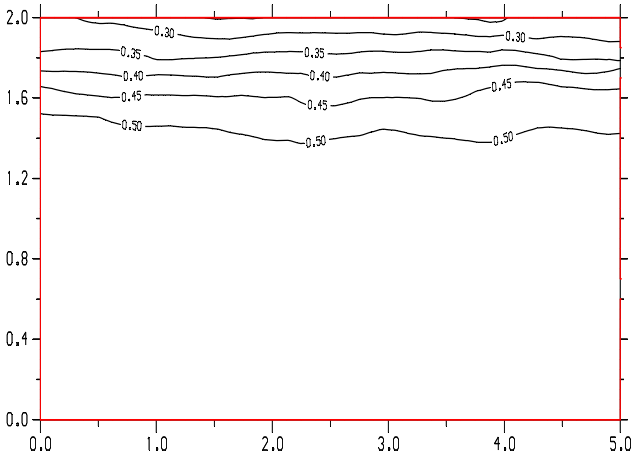

(b) Concentration profile at $y = 2.5$ m after 1.25 days: simulation B5

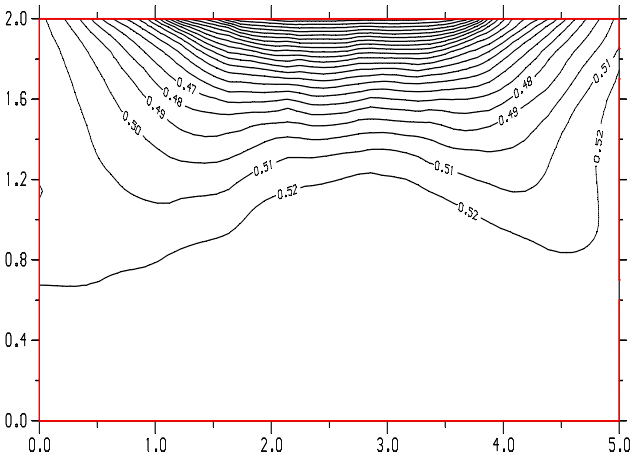

(c) Concentration profile at $y = 2.5$ m after 1.25 days: simulation B6

Figure 5.18: Concentration profiles from heterogeneous Set 2 simulations

5.5 Comparison of Results to Previous Studies

Though no research was found involving the injection of a dense brine at points in a domain, comparisons between brine emplacement results and density-dependent-flow literature can be made. As suggested by previous research, the dense brine did form mounds on the impermeable clay surface, and the amount of mounding that occurred was dependent on subsurface heterogeneity and fluid velocity [53]. In a density dependent flow experiment employing layered media, Schincariol and Schwartz observed that as the number of layers increased, the flow and transport of a dense plume began to more closely resemble that seen in homogeneous experiments [53]. In the present study, this generalization was not valid, as evidenced by analysis of simulation E6. Over a height of 3.2 meters, 46 layers were utilized—an amount that would imply resultant behavior representative of that in the homogeneous simulations. Yet, the presence of a low permeability layer near the clay surface caused instabilities to form and resulted in concentration profile patterns which varied greatly from all other simulations. This is, however, in accordance with Simmons et al., who demonstrated that local heterogeneities, as opposed to permeability field statistics, determine instability patterns [57]. The ln permeability field used in simulation E6, as well as resulting concentration profiles, can be seen in Figures 5.19(a) and 5.19(b).

Brine recovery simulations further verify theory found in the literature that flow and transport are greatly dependent on the cumulative distribution of high and low permeability areas [57]. Though the efficiency of solute removal did not depend on the variance of the permeability field, the specific heterogeneous domain was the greatest factor in the amount of solute removed. In addition, instabilities were seen to form in both the LF and UF simulations, as freshwater displaced a dense brine. These instabilities, portrayed previously in Figures 5.11(a) and 5.11(b), were expected, based on previous investigations of density dependent flow. Though not quantified in this study, complex velocity profiles were observed in brine recovery simulations. This is

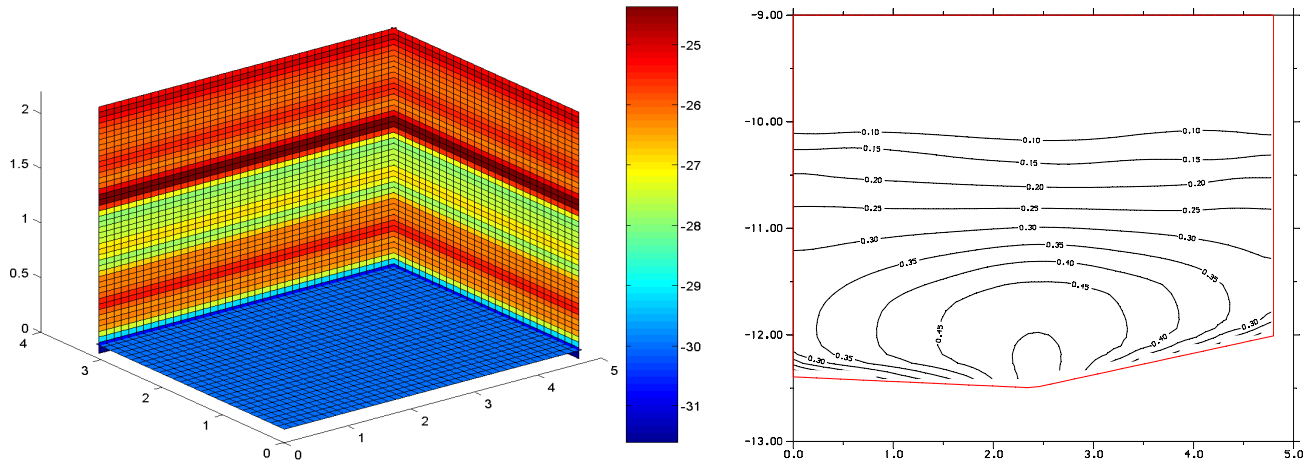

(a) *ln* permeability field, profile of (4.7,3.1,0.1) meters: Simulation E6

(b) Concentration profile at $y = 0.1$ m after 16 days: simulation E6

Figure 5.19: *ln* permeability fields and concentration profiles: Simulation E6

in agreement with various studies in which small density differences led to mixing [10, 52, 56, 57]. However, it can not be determined whether complex flow fields in simulations were a result of density differences, heterogeneity, or simply the combination of fluid injection and extraction.

In all viscosity simulations, the negligence of viscosity variations led to an overestimation of both horizontal and downward vertical velocities. In homogeneous Set 1 simulations, the final horizontal velocity was overestimated by 0.12 m day^{-1}, and the vertical velocity by 2.04 m day^{-1}. In homogeneous Set 2 simulations, the horizontal and vertical velocities were overestimated by 1.47 m day^{-1} and 3.63 m day^{-1}, respectively. This supports Ophori's hypothesis that an underestimation of viscosity leads to an overestimated prediction of groundwater sinking [44]. More importantly, it demonstrates the importance of accounting for viscosity variations when modeling systems containing a dense and viscous brine.

Set 1 viscosity simulations also demonstrated an effect observed by Schincariol and Schwartz. In laboratory experiments, they observed that a dense plume moved horizontally in freshwater at a much greater velocity than that of a low density injection [53]. In viscosity simulations in which brine displaced freshwater, the final horizontal velocity of the dense brine was 0.34 m day^{-1} greater than the non-dense brine in homogeneous simulations and 0.12 m day^{-1} greater in heterogeneous simulations.

Though performed to evaluate the effects of viscosity on brine behavior, the Set 1 and Set 2 viscosity simulations also further demonstrated the significant effect that heterogeneity has on fluid velocities. On average, the velocity in heterogeneous simulations was 33% smaller than that seen in corresponding homogeneous simulations. Though only one correlated random permeability field was used in the viscosity simulations, and a relationship between velocity and heterogeneity can not be made, it is obvious that subsurface heterogeneity impacts fluid flow and solute transport.

6 Conclusions

As DNAPL contamination continues to be a challenge to groundwater remediation efforts, a novel brine barrier approach is being tested in the laboratory, as well as at the field-scale. Though experiments have addressed the effects of subsurface heterogeneity on its efficiency, a more comprehensive study is afforded by mathematical modeling. The objective of this project was to utilize a numerical model to investigate open issues relating to BBRT—specifically, the effects of heterogeneity and viscosity on brine behavior.

Simulations showed highly viscous $CaBr_2$ to form mounds around injection wells when introduced into a freshwater-saturated domain. However, the use of a moderate rate of brine emplacement was able to control the amount of mounding that occurred and to limit the amount of mass which dispersed upward into the domain. Highly heterogeneous domains resulted in an insufficient brine barrier establishment over the simulation period. However, among moderately heterogeneous domains, the subsurface variation was less dominant a factor in brine emplacement efficiency than was the injection rate.

Contrary to results found in brine emplacement analysis, the efficiency of brine recovery was seen to depend strongly on subsurface heterogeneity and be a weak function of extraction rate. Though the variance of the permeability field was not indicative of overall efficiency, local heterogeneities were the dominant factor in fractional solute recovery. Therefore, it is beneficial to have a knowledge of the subsurface prior to implementation, as this information will help determine the feasibility of BBRT.

The present study demonstrated the promise of BBRT and suggested methods of increasing the efficiency of brine emplacement and recovery. However, concerns were raised on the applicability of many groundwater flow and transport models, especially those in which a homogeneous

domain and constant viscosity are assumed. Accounting for the subsurface variability was shown to be essential, as it may determine whether BBRT is appropriate for a specific domain. In addition, viscosity simulations demonstrated inaccuracies caused by neglecting viscosity variations, as they were seen to significantly affect fluid velocities.

To better understand the processes involved in BBRT, further research should be conducted on the dispersion of brine. Though diffusion observed in laboratory experiments is best estimated by a coefficient twice that of the published value for $CaBr_2$, the overall effects of hydrodynamic dispersion have yet to be studied. Specifically, the proposed non-linear dispersion theory should be investigated on its applicability to a dense brine. It is possible that non-linear dispersion effects may counteract the effects of viscosity by dispersing mounds.

References

[1] P. Ackerer, A. Younes, and R. Mose. Modeling variable density flow and solute transport in porous medium I. Numerical model and verification. *Transport in Porous Media*, 35: 345–373, 1999.

[2] J. J. Adams and S. Bachu. Equations of state for basin geofluids: Algorithm review and intercomparison for brines (vol 2, pg 257, 2002). *Geofluids*, 4(3):250, 2004.

[3] J. Bear. *Dynamics of Fluids in Porous Media*. Elsevier, New York, 1972.

[4] J. Bear. *Hydraulics of Groundwater*. McGraw-Hill, New York, 1979.

[5] S. F. Carle and G. E. Fogg. Transition probability-based indicator geostatistics. *Mathematical Geology*, 28(4):453–476, 1996.

[6] L. R. Chevalier, S. J. Masten, R. B. Wallace, and D. C. Wiggert. Experimental investigation of surfactant-enhanced dissolution of residual NAPL in saturated soil. *Ground Water Monitoring and Remediation*, 17(4):89–98, 1997.

[7] G. Dagan. Comment on 'A note on the recent natural gradient tracer test at the borden site' by R. L. Naff, T.-C. Jim Yeh, and M. W. Kemblowski. *Water Resources Research*, 25 (12):2521–2522, 1989.

[8] M. Dekking, A. Elfeki, C. Kraaikamp, and J. Bruining. Multi-scale and multi-resolution stochastic modeling of subsurface heterogeneity by tree-indexed Markov chains. *Computational Geosciences*, 5(1):47–60, 2001.

[9] C. V. Deutsch and A. G. Journel. *GSLIB: Geostatistical Software Library and User's Guide*. Oxford University Press, New York, 1992.

[10] H. J. G. Diersch and O. Kolditz. Variable-density flow and transport in porous media: Approaches and challenges. *Advances in Water Resources*, 25(8-12):899–944, 2002.

[11] H. J. G. Diersch and O. Kolditz. Coupled groundwater flow and transport: 2. Thermohaline and 3D convection systems. *Advances in Water Resources*, 21:401–425, 1998.

[12] F. W. Domenico and P. A. Schwartz. *Physical and Chemical Hydrogeology*. John Wiley & Sons, Inc., New York, 1998.

[13] T. T. Eaton. On the importance of geological heterogeneity for flow simulation. *Sedimentary Geology*, 184(3–4):187–201, 2006.

[14] A. Elfeki and M. Dekking. A markov chain model for subsurface characterization: Theory and applications. *Mathematical Geology*, 33(5):569–589, 2001.

[15] E. V. Fitchett. An investigation of residual coal tar mobilization in water saturated porous media. Technical report, University of North Carolina at Chapel Hill, Chapel Hill, NC, 2004.

[16] R. A. Freeze. A stochastic-conceptual analysis of one-dimensional groundwater flow in nonuniform homogeneous media. *Water Resources Research*, 11(5):725–741, 1975.

[17] J. J. Fried. Groundwater pollution. In J. J. Fried, editor, *The Experimental Determination of Groundwater Pollution Parameters*, pages 59–113. Elsevier Scientific Publishing Co., Amsterdam, 1975.

[18] W. D. Graham and D. B. McLaughlin. A stochastic model of solute transport in groundwater: Application to the Borden, Ontario, tracer test. *Water Resources Research*, 27(6): 1345–1359, 1991.

[19] S. M. Hassanizadeh. Derivation of basic equations of mass transport in porous media, part 2. Generalized Darcy's and Fick's laws. *Advances in Water Resources*, 9(4):207–222, 1986.

[20] S. M. Hassanizadeh. Derivation of basic equations of mass transport in porous media, part 1. Macroscopic balance laws. *Advances in Water Resources*, 9:196–206, 1986.

[21] S. M. Hassanizadeh. Modeling species transport by concentrated brine in aggregated porous media. *Transport in Porous Media*, 3(3):299–318, 1988.

[22] S. M. Hassanizadeh and A. Leijnse. A non linear theory of high-concentration-gradient dispersion in porous media. *Advances in Water Resources*, 18(4):203–215, 1995.

[23] S. M. Hassanizadeh and T. Leijnse. On the modeling of brine transport in porous media. *Water Resources Research*, 24(3):321–330, 1988.

[24] E. H. Hill, M. Moutier, J. Alfaro, and C. T. Miller. Remediation of DNAPL pools using dense-brine barrier strategies. *Environmental Science & Technology*, 35(14):3031–3039, 2001.

[25] E. H. Hill, L. L. Kupper, and C. T. Miller. Evaluation of path-length estimators for characterizing multiphase systems using polyenergetic X-ray absorptimetry. *Soil Science*, 167(11): 703–719, 2002.

[26] G. M. Homsy. Viscous fingering in porous media. *Ann. Rev. Fluid Mech.*, 19:271–311, 1987.

[27] P. T. Imhoff and C. T. Miller. Dissolution fingering during the solubilization of nonaqueous phase liquids in saturated porous media 1. Model predictions. *Water Resources Research*, 32(7):1919–1928, 1996.

[28] P. T. Imhoff, G. P. Thyrum, and C. T. Miller. Dissolution fingering during the solubilization of nonaqueous phase liquids in saturated porous media 2. Experimental observations. *Water Resources Research*, 32(7):1929–1942, 1996.

[29] D. N. Johnson, J. A. Pedit, and C. T. Miller. Efficient, near-complete removal of DNAPL from three-dimensional, heterogeneous porous media using a novel combination of treatment technologies. *Environmental Science & Technology*, 38(19):5149–5156, 2004.

[30] R. Juanes and M. J. Blunt. Analytical solutions to multiphase first-contact miscible models with viscous fingering. *Transport in Porous Media*, 64:339–373, 2006.

[31] V. Kapoor and L. W. Gelhar. Transport in 3-Dimensionally heterogeneous aquifers .2. Predictions and observations of concentration fluctuations. *Water Resources Research*, 30 (6):1789–1801, 1994.

[32] C. Knudby, J. Carrera, J. D. Bumgardner, and G. E. Fogg. Binary upscaling—-the role of connectivity and a new formula. *Advances in Water Resources*, 49:590—604, 2006.

[33] M. Koch and G. Zhang. Numerical simulation of the migration of density dependent contaminant plumes, SCRI. Technical report, Florida Department of Environmental Regulation, Florida State University, Tallahassee, FL, 1991.

[34] M. Koch and G. Zhang. Numerical simulation of the effects of variable density in a contaminant plume. *Ground Water*, 30(5):731–742, 1992.

[35] D. A. Lever and C. P. Jackson. On the equations for the flow of concentrated salt solution through a porous medium. Technical Report DOE Report No: DOE/RW/85.100 DOE Reference: PECD-7/9/230/86/84 Contractor's Reference: AERE-R.11765, United Kingdom Atomic Energy Authority, Publications Office, Harwell Laboratory, Oxfordshire, England, 1985.

[36] S. L. Lu, F. J. Molz, G. E. Fogg, and J. W. Castle. Combining stochastic facies and fractal models for representing natural heterogeneity. *Hydrogeology Journal*, 10(4):475–482, 2002.

[37] T. McGuire, J. McDade, and C. Newell. Performance of DNAPL source depletion technologies at 59 chlorinated solvent-impacated sites. *Ground Water Monitoring and Remediation*, 26(1):73–84, 2006.

[38] R. McKibbin and O. S. M.J. Onset of convection in a layered porous medium heated from below. *Journal of Fluid Mechanics*, 96:375–393, 1980.

[39] C. T. Miller. Remediation of DNAPL-contaminated subsurface systems. In *Annual Quadrangle Conference on Environmental Sciences and Engineering*, Blacksburg, VA, 1999.

[40] C. T. Miller, S. N. Gleyzer, and P. T. Imhoff. Numerical modeling of NAPL dissolution fingering in porous media. In H. M. Selim and L. Ma, editors, *Physical Nonequilibrium in Soils: Modeling and Application*. Ann Arbor Press, Ann Arbor, MI, 1998.

[41] C. T. Miller, E. H. Hill, and M. Moutier. Remediation of DNAPL-contaminated subsurface systems using density-motivated mobilization. *Environmental Science & Technology*, 34(4): 719–724, 2000.

[42] C. T. Miller, M. W. Farthing, C. E. Kees, and C. T. Kelley. Higher order locally conservative temporal integration methods for modeling multiphase flow in porous media. In S. M. Hassanizadeh, R. J. Schotting, W. G. Gray, and G. F. Pinder, editors, *XIV International Conference on Computational Methods in Water Resources*, volume Developments in Water Science, 47, Computational Methods in Water Resources, Volume 1, pages 249–256, Delft, The Netherlands, 2002. Elsevier.

[43] C. M. Oldenburg and K. Pruess. Dispersive transport dynamics in a strongly coupled groundwater brine flow system. *Water Resources Research*, 31(2):289–302, 1995.

[44] D. U. Ophori. The significance of viscosity in density-dependent flow of goundwater. *Journal of Hydrology*, 204:261–270, 1998.

[45] C. Paniconi and M. Putti. A comparison of Picard and Newton iteration in the numerical solution of multidimensional variably saturated flow problems. *Water Resources Research*, 30(12):3357–3374, 1994.

[46] A. Prasad and C. T. Simmons. Unstable density-driven flow in heterogeneous porous media: A stochastic study of the elder [1967b] "short heater" problem. *Water Resources Research*, 39(1):1–21, 2003.

[47] A. M. Provost. Sutraprep: A preprocessor for SUTRA, a model for ground-water flow with solute or energy transport. Technical report, United States Geological Survey, Reston, VA, 2003.

[48] L. Rayleigh. On convection currents in a horizontal layer of fluid when the higher temperature is on the under side. *Philos. Mag.*, 6(32):529–546, 1916.

[49] The RETEC Group Inc and The University of North Carolina at Chapel Hill. Technology demonstration work plan for brine-based remediation technologies. Technical report, Dover National Test Cite, Dover Air Force Base, Delaware, 2005.

[50] Y. Rubin. *Applied Stochastic Hydrogeology*. Oxford University Press, Oxford,NY, 2003.

[51] B. R. Scanlon, R. E. Mace, M. E. Barrett, and B. Smith. Can we simulate regional groundwater flow in a karst system using equivalent porous media models? Case study, Barton Springs Edwards Aquifer, USA. *Journal of Hydrology*, 276:137–158, 2003.

[52] R. A. Schincariol. Dispersive mixing dynamics of dense miscible plumes: natural perturbation initiation by local-scale heterogeneities. *Journal of Contaminant Hydrology*, 34:247–271, 1998.

[53] R. A. Schincariol and F. W. Schwartz. An experimental investigation of variable density flow and mixing in homogeneous and heterogeneous media. *Water Resources Research*, 26 (10):2317–2329, 1990.

[54] R. J. Schotting, H. Moser, and S. M. Hassanizadeh. High-concentration-gradient dispersion in porous media: Experiments, analysis and approximations. *Advances in Water Resources*, 22(7):665–680, 1999.

[55] S. G. Shikaze, E. A. Sudicky, and F. W. Shchwartz. Density-dependent solute transport in discretely-fractured geologic media: is prediction possible? *Journal of Contaminant Hydrology*, 34:273–291, 1998.

[56] C. T. Simmons and K. A. Narayan. Mixed convection processes below a saline disposal basin. *Journal of Hydrology*, 194:263–285, 1997.

[57] C. T. Simmons, T. R. Fenstemaker, and J. M. Sharp. Variable-density groundwater flow and solute transport in heterogeneous porous media: approaches, resolutions, and future challenges. *Journal of Contaminant Hydrology*, 52:245–275, 2001.

[58] L. Smith and R. A. Freeze. Stochastic analysis of steady state groundwater flow in a bounded domain: 1. One-dimensional simulations. *Water Resources Research*, 15(3):521–528, 1979.

[59] W. R. Souza. Sutraplot: A graphical post-processor for SUTRA, a model for ground-water flow with solute or energy transport. Technical report, United States Geological Survey, Reston, VA, 2003.

[60] E. A. Sudicky. A natural gradient experiment on solute transport in a sand aquifer: Spatial variability of hydraulic conductivity and its role in the dispersion process. *Water Resources Research*, 22(13):2069–2082, 1986.

[61] R. A. Trompert, J. G. Verwer, and J. G. Blom. Computing brine transport in porous media with an adaptive-grid method. *International Journal for Numerical Methods in Fluids*, 16 (1):43–63, 1993.

[62] C. I. Voss and A. M. Provost. SUTRA: A model for saturated-unsaturated variable-density ground-water flow with solute or energy transport. Technical report, U.S. Geological Survey, Reston, VA, 2002.

[63] G. S. Weissmann and G. E. Fogg. Multi-scale alluvial fan heterogeneity modeled with transition probability geostatistics in a sequence stratigraphic framework. *Journal of Hydrology*, 226:48–65, 1999.

[64] R. Wen. Multi-scale heterogeneity modeling–A method of reservoir data integration. In *Geomodeling*, Vienna, 2006.

[65] X. H. Wen and J. J. Gḿez-Hernńdez. Upscaling hydraulic conductivities in heterogeneous media: An overview. *Journal of Hydrology*, 183(1/2):ix, 1996.